TEMPERATURE AND WELL-WIDTH DEPENDENCE OF PHOTOLUMINESCENCE TRANSITIONS IN AN AlGaAs/GaAs MQW SAMPLE

A Thesis Presented to
The Department of Physics at
Western Illinois University
In Partial Fulfillment of
The Requirements for
The Honors Degree
Bachelor of Science

By
Daniel A. Johnson
Spring 2001

ABSTRACT OF THESIS

The heavy and light hole transitions of an MBE (Molecular-Beam-Epitaxy) grown Al (0.3) Ga (0.7) As / GaAs MQW (Multiple Quantum Well) sample were investigated over a temperature range of 20-300 K using the technique of photoluminescence. The MQW sample contained GaAs wells of widths 47 Å, 70 Å, 93 Å, 117 Å and 140 Å sandwiched between AlGaAs barriers of >500Å. Because the bandgap of GaAs (1.4 eV) is less than that of the AlGaAs (1.8 eV), the electron-hole recombinations take place almost entirely within the one-dimensional quantum wells formed by the narrow layers of GaAs. The MQW sample was illuminated with the 4880 Å line of an Argon-Ion Laser with an incident power at the sample surface of approximately 20mW. The sample was mounted on a cold head and its temperature controlled with a closed-cycle Leybold helium refrigeration system and monitored by a Lakeshore platinum resistor. The photoluminescence spectra were collected using an automated single grating (1200 grooves/mm) Triax 550 spectrometer equipped with a GaAs PMT (photo-multiplier tube) and controlled with LabView data acquisition software. The temperature dependence of all transition energies was found to closely follow the conventional GaAs empirical equation for temperature dependence. In addition, the transition energies appropriately scaled as the inverse square of the well-width, as predicted from one-dimensional quantum mechanical theory, except for slight departure at very narrow well widths.

This thesis is accepted in its present form as satisfying the requirements for the honors degree of Bachelor of Science in Physics.

_____

Honors Thesis Supervisor, Dr. Mark S. Boley

_____

Date Approved

Table of Contents

List of Figures…….5

Introduction and Background Theory……8

Experimental Procedure……...……....14

Results and Discussion…….16

Conclusion……20

Acknowledgments……21

References……...…….22

Tables and Figures……23

List of Figures and Tables

Tables Page#

1. Energy Predictions for Light and Heavy…….23
   Holes for the 5 Wells at T=0K

Figure

1. Schematic of Multiple Quantum Well Sample……24
2. GaAs Direct Bandgap Transition Diagram…….25
3. Infinite Square Well Energies and Quantum …….26
   Numbers
4. Schematic of Experimental Apparatus……27
5. Plot of Raw Data With Light and ……..….28
   Heavy Hole Peaks Labeled Taken at T=21K
6. Plot of Raw Data With Light and ……..…..29
   Heavy Hole Peaks Labeled Taken at T=37K
7. Close Up Plot of Raw Data With Light and ……...30
   Heavy Hole Peaks Labeled Taken at T=37K
8. Plot of Raw Data With Light and ……...31
   Heavy Hole Peaks Labeled Taken at T=53K
9. Close Up Plot of Raw Data With Light and ……...32
   Heavy Hole Peaks Labeled Taken at T=53K
10. Plot of Raw Data With Light and ……...33
    Heavy Hole Peaks Labeled Taken at T=75K
11. Close Up Plot of Raw Data With Light and ……...34
    Heavy Hole Peaks Labeled Taken at T=75K
12. Plot of Raw Data With Light and …….……...35
    Heavy Hole Peaks Labeled Taken at T=100K
13. Close Up Plot of Raw Data With Light and……36
    Heavy Hole Peaks Labeled Taken at T=100K
14. Plot and Close Up of Raw Data With Light and …….37
    Heavy Hole Peaks Labeled Taken at T=125K
15. Plot of Raw Data With Light and……38
    Heavy Hole Peaks Labeled Taken at T=150K
16. Close Up Plot of Raw Data With Light and……39
    Heavy Hole Peaks Labeled Taken at T=150K
17. Plot of Raw Data With Light and……40
    Heavy Hole Peaks Labeled Taken at T=175K

18. Close Up Plot of Raw Data With Light and……41
Heavy Hole Peaks Labeled Taken at T=175K
19. Plot of Raw Data With Light and……42
Heavy Hole Peaks Labeled Taken at T=200K
20. Plot of Raw Data With Light and……43
Heavy Hole Peaks Labeled Taken at T=220K
21. Plot of Raw Data With Light and……44
Heavy Hole Peaks Labeled Taken at T=241K
22. Plot of Raw Data With Light and……45
Heavy Hole Peaks Labeled Taken at T=270K
23. Plot of Raw Data With Light and……46
Heavy Hole Peaks Labeled Taken at T=291K
24. Plot and Linear Fit of Energy vs. Inverse Square……47
Of Well Width for Heavy Holes at T=21K
25. Plot and Linear Fit of Energy vs. Inverse Square……48
Of Well Width for Heavy Holes at T=37k
26. Plot and Linear Fit of Energy vs. Inverse Square……49
Of Well Width for Heavy Holes at T=53k
27. Plot and Linear Fit of Energy vs. Inverse Square……50
Of Well Width for Heavy Holes at T=75K
28. Plot and Linear Fit of Energy vs. Inverse Square……51
Of Well Width for Light Holes at T=75K
(Note this is the mininum termperature at which
the light holes could be fit with certainty)
29. Plot and Linear Fit of Energy vs. Inverse Square……52
Of Well Width for Heavy Holes at T=100K
30. Plot and Linear Fit of Energy vs. Inverse Square……53
Of Well Width for Light Holes at T=100K
31. Plot and Linear Fit of Energy vs. Inverse Square……54
Of Well Width for Heavy Holes at T=125K
32. Plot and Linear Fit of Energy vs. Inverse Square…....55
Of Well Width for Light Holes at T=125K
33. Plot and Linear Fit of Energy vs. Inverse Square……56
Of Well Width for Heavy Holes at T=150K
34. Plot and Linear Fit of Energy vs. Inverse Square……57
Of Well Width for Light Holes at T=150K
35. Plot and Linear Fit of Energy vs. Inverse Square……58
Of Well Width for Heavy Holes at T=175K

36. Plot and Linear Fit of Energy vs. Inverse Square……59
Of Well Width for Light Holes at T=175K
37. Plot and Linear Fit of Energy vs. Inverse Square……60
Of Well Width for Light annd Heavy Holes at
T=200K
38. Plot and Linear Fit of Energy vs. Inverse Square……61
Of Well Width for Light Holes at T=220K
39. Plot and Linear Fit of Energy vs. Inverse Square……62
Of Well Width for Heavy Holes at T=220K
40. Plot and Linear Fit of Energy vs. Inverse Square……63
Of Well Width for Heavy Holes at T=241K
41. Plot and Linear Fit of Energy vs. Inverse Square……64
Of Well Width for Light Holes at T=241K
42. Plot and Linear Fit of Energy vs. Inverse Square……65
Of Well Width for Heavy Holes at T=270K
43. Plot and Linear Fit of Energy vs. Inverse Square……66
Of Well Width for Light Holes at T=270K
44. Plot and Linear Fit of Energy vs. Inverse Square……67
Of Well Width for Heavy Holes at T=291K
45. Plot and Linear Fit of Energy vs. Inverse Square……68
Of Well Width for Light Holes at T=291K
46. Plots and Curve Fits of Energy vs. Temperature…….69
For Light and Heavy Holes for the 5 Wells

INTRODUCTION AND BACKGROUND THEORY:

Through the application of Molecular-Beam-Epitaxy (MBE) technology a multiple quantum well (MQW) sample was created at Purdue University and was granted to us by the University of Missouri-Columbia for the purposes of this study. The purpose of this experiment was threefold: to study the temperature and the well width dependence of the emitted photon energies from electron-hole recombinations excited by photoluminescence transitions that occur in the MQW sample, and to also test and calibrate the Western Illinois University Physics Department's spectroscopy lab. The physics governing the quantum well's behavior and the motion of its electrons and holes along with their transition energies is found in the field of quantum mechanics and is modeled according to its rules.

Technology today has given mankind control over matter to an extent that he has never before known. MBE allows us to grow materials nearly atom by atom. These materials can be designed to study specific quantum mechanical situations in an experimental setting. This is very useful in the world of computing where the size of circuitry has already entered the realm where the rules of quantum mechanics come into play. This technique has also allowed the fabrication of quantum well lasers, quantum dot superlattices, and other quantum optical devices. A simple and more fundamental quantum mechanical example that can be created by MBE is the finite square well. Using semi-conducting materials of different band-gaps and grown in layers by MBE,

materials can be specifically designed to create one dimensional quantum confinement areas, approximately simulating the textbook one-dimensional infinite (see Figure 3) or finite square wells.

The sample itself is composed of $Al_{0.3}Ga_{0.7}As$ and GaAs, where the GaAs is used to create the layers in which the observable electron-hole recombinations occur, that is, the quantum confinement areas for electrons and holes. The promotion of electrons from the valence band to the conduction band occurs in both AlGaAs and GaAs due to the absorption of the laser photons of energies higher then the bandgap in either material; however, the recombinations within the AlGaAs have a low probability and would be unobservable, due to the material's indirect band gap that prevents the photon from being directly ejected during a potential electron-hole recombination. Therefore most of the electrons and holes cascade into the GaAs quantum confinement areas (wells) via slow phonon interactions prior to their direct bandgap recombination in the GaAs, which can be observed by the corresponding emission of photons from this GaAs layer.

From Figure 1 it can be seen that the sample was grown along the z-axis with the narrowest wells closest to the surface of the sample in order to prevent their higher-energy transition photons from being absorbed by the larger wells, which have lower-energy transitions. The narrowest wells are transparent to the photons emitted from the widest wells since these photons would have insufficient energy to promote an electron from the valence band to the

conduction band in the narrower wells. The widths of the wells in the MQW sample are specifically designed and are precisely controlled so that they are known to within ± 2Å. The five wells are of widths 47Å, 70Å, 93Å, 117Å and 140Å with AlGaAs separation layers of width greater then 500Å to minimize the interaction between the wells due to quantum periodicity effects. The depths of the wells are not great enough to observe transitions between energy levels with quantum numbers greater than 1, since the existence of energy levels with n=2 in the quantum wells would require well depths of at least 4 times the energy of the n=1 levels due to the dependence of energy upon the square of n, and our wells are likely not that deep. Recall that

$$E = \frac{n^2 h^2}{8ml^2} \tag{1}$$

for the one-dimensional square well formula. The multiple wells in our sample are essential to the study of the dependence of the electron-hole recombination energies on well width.

Without the presence of the quantum wells the electron-hole recombinations would be seen as one large peak with energy slightly below the bandgap of the material, and the light-hole recombinations would be masked by the heavy-hole recombinations and would occur at almost exactly the same transition energy. It is the dependence of quantum confinement energy on mass that allows us to separate the light- and heavy-hole transition energies. The

quantum wells allow for a far more precise knowledge of the position of the electrons in the sample and due to the Heisenberg Uncertainty Principle,

$$\Delta x \Delta p \geq \frac{h}{4\pi} \tag{2}$$

the momentum of the electrons, as well as their corresponding transition energies, will now become greater, and the light- and heavy-hole transition energies will now become separated and distinguishable due to quantum confinement.

Formation of electron-hole pairs and their recombinations occur readily in GaAs and are easily observable due to GaAs's direct bandgap (see Figure 2). AlGaAs's band gap is indirect and is therefore used to make the barriers of the quantum well where very few transitions will occur. The bandgap of GaAs is 1.4 eV and is therefore easily detectable using the technique of optical spectroscopy in the visible range or the near IR range. As the laser photons are absorbed, electrons are promoted to the conduction band, leaving holes (the absence of electrons) behind in the valence band. When holes recombine with electrons, a photon is then emitted, resulting in luminescence from the material. There is a distinction between the types of holes created and their effective mass differences; light and heavy, distinguish them, where the light holes have the higher mobility and greater energy. In figure 2, the different curvatures for the light and heavy holes correspond to their differences in effective mass, which is

related to the k-space dependence of energy by the equation

$$m^* \propto \frac{1}{d^2E/dk^2} \qquad (3).$$

The holes reside in the valence band due to the promotion of the electrons to the conduction band in response to the laser photons, hence the name *photo*luminescence. The electrons then reside in the conduction band until they cascade back down to the lower energy band and recombine with the holes, emitting a photon in this process. The photon energies corresponding to the recombination of electrons and holes are the energies seen in the photoluminescence spectra, and correspond to

$$E_{bandgap(GaAs)} + E_{light-hole(n=1)} + E_{electron(n=1)} \qquad (4)$$

for the light hole case and to

$$E_{bandgap(GaAs)} + E_{heavy-hole(n=1)} + E_{electron(n=1)} \qquad (5)$$

for the heavy hole case. Thus it is the summation of the quantum confinement energies for electrons and holes and the bandgap energy of GaAs that will determine the locations in energy of the light-hole and heavy-hole peaks in the photoluminescence (PL) spectra. When observing the transitions as peaks of energy in the PL spectra, the intensities of the light holes are less then that of the heavy holes due to the fact that they occur at higher energy, and the Boltzmann thermal factor (e^{-kt}) causes a lower population level in the light-hole energy

levels then in the lower heavy-hole energy levels. Note these levels are different primarily due to the quantum confinement in the GaAs well regions.

The model that was used to predict the behavior of the energy levels within the wells was the infinite square well approximation (see Figure 3), although it was known beforehand that the wells would not truly behave as the infinite square well. Due to the lack of detailed information about the wells' edges and exact depths, it would be impossible to effect any meaningful improvements in the data analysis and fitting using the numerical techniques required for the finite square well approximation.

EXPERIMENTAL PROCEDURE:

The experimental procedure and setup are illustrated in Figure 4 and will be outlined in the following explanation.

The setup began with the source of excitation photons, which is an Argon-Ion laser operating with an output power of approximately 0.5 Watts at 488.0 nm. The selection of that wavelength was due to the availability in our laboratory of optical line filters and super notch filters designed for 488.0 nm. To decrease the intensity of the emitted beam so as not to damage the sample surface or overpower the photo-multiplier tube (PMT) with too large of a sample luminescence signal, a series of neutral density filters was used. At the beginning of this experiment there was no proper holder for the neutral density filters. Consequently, as part of this honors project, a Teflon mount to hold securely and level up to 8 filters was constructed to address this problem. Teflon was used to prevent scratching and increase the ease of sliding the filters in and out of the beam line.

After passing through the neutral density filters the beam was then reflected via a series of mirrors to the proper height at which the sample and spectrometer reside. The beam then travels through a 488.0 nm line filter where all plasma emissions and other energies of laser emission are then filtered out. A prism mirror is then used to reflect the beam into the sample mount. The selection of a prism mirror was chosen because the face of the mirror is on the order of the cross sectional area of the laser beam, allowing for minimum

shadowing or blocking of the emitted luminescence from the sample, which needs to be maximally collected by the spectrometer. The sample is mounted within a cold head apparatus, which is evacuated via a roughing pump, and cooled to cryogenic temperatures via a closed cycle helium refrigeration (Leybold) system. This allows the sample to reach temperatures as low as 20 K, with a Lakeshore platinum resistor monitoring the sample temperature at all times. The emissions from the sample are then collected and focused onto the entrance slit of the spectrometer with a series of high quality focusing lenses. The spectrometer is a single grating (1200 grooves/mm) fully automated Triax 550 equipped with a GaAs PMT, which has a maximum sensitivity in the region of interest for our transitions. The data is then collected using an in-house-created virtual instrument written and controlled within National Instrument's LabView software. Microsoft Excel was used for all of the data plotting, curve fitting, and data analysis.

RESULTS AND DISCUSSION:

Once the data was taken from LabView it was transferred into Excel; and after plotting, all of the peaks were labeled and identified by their energy in electron volts, by their wavelength in nanometers, and by the type of recombination, light-hole or heavy-hole, that gave rise to that peak in the PL spectra (Figures 5-23). The wavelengths of the peaks were then converted into values of energy using the relationship:

$$E = \frac{hc}{\lambda} \tag{6}$$

where *E* is the energy, *h* is Plank's constant, *c* is the speed of light, and λ is the wavelength of the photon. For this calculation, the value of *hc* was used as 1240 eV-nm.

Once the energies had been identified and tabulated, they were then plotted versus the inverse square of well width at each temperature for which PL spectra were collected (the temperatures being: 21K, 37K, 53K, 75K, 100K, 125K, 150K, 175K, 200K, 220K, 241K, 270K and 291K), as can be seen in Figures 24-45. Using least squares fitting it could be seen that the relationship between the transition energy and the inverse square of well width tracked almost linearly, as predicted by the infinite square well approximation

$$E = \frac{h^2 n^2}{8ml^2} \tag{1}$$

where *n* is the quantum number, *h* is Plank's constant, *m* is the effective mass of the electron or of the light- or heavy-holes, and *l* is the width of the quantum

well. This approximation worked well for the widest quantum wells, but failed to accurately fit the narrowest (47Å) well. Obviously, a dramatic improvement in the fit is observed after the narrowest well values are removed from the data set for the linear least squares fitting. This was verified by the correlation coefficients for the differing 4- and 5-well fits; the 5-well fit's coefficient of 0.9831 is not nearly as high in quality as the 4-well fit's coefficient of 0.9964 for the data at 100K (see Figure 29), where a value of 1 would imply a perfect correlation and a value of 0 would imply no relation between the data and the fit. This fitting failure for the narrowest well was due to the electrons' and holes' abilities to quantum tunnel through the walls of the well, since the 47Å well is closest in size to the deBroglie wavelength of the electron. In addition, the narrowest well would be expected to have the largest percentage impact of tunneling effects due to the higher energies of electrons and holes in that well. As expected, the plotted light holes were seen to be at a higher energy then the heavy holes, and also failed to be linearly fit at the narrowest well width, for the same reasons as explained above.

The dependence of the transitions' energies upon temperature was plotted for each of the quantum well's photoluminescent heavy-hole transitions and for the light-hole transitions occurring in the 47 Å, 70 Å, and 93 Å quantum

wells as shown in Figure 46. The light-hole transitions were masked by the heavy hole transitions in the wider wells. The energies were fitted using the accepted equation for the dependence of the bandgap of GaAs on temperature, knowing that the observable electron-hole recombinations occurred within the GaAs layers, due to its direct band gap and due to the quantum confinement within these regions. This equation is

$$E = E(T = 0K) - \frac{\alpha T^2}{\beta - T} \tag{7}$$

where α and β are material constants for GaAs, which are readily found in the literature, corresponding to α = 5.4x10^{-4} eV and β = 204 K. Obviously, the confinement energies of the electrons and the holes were not assumed to be temperature-dependent, a conclusion that was borne out by the quality of the curve fittings seen in Figure 46. From this fit the value of the photon energies can be predicted at 0K, which was the adjustable parameter in the temperature fits, and the values are assembled in Table 1. Knowing this value for energy the effective masses of the light and heavy holes can also be calculated. This calculation begins with

$$\Delta E = 1.4eV + E_{electron} + E_{hole\,(light\,/\,heavy)} \tag{9}$$

where the value of 1.4 eV is the bandgap of GaAs and ΔE is the value predicted for the photon energy at 0K. Next we apply the quantum confinement equation,

$$E_{electron} = \frac{h^2 n^2}{8m^* l^2} \tag{10}$$

which is used to find the value of $E_{electron}$, where m^* is taken to be the effective mass of the electron given for GaAs as $0.06m_e$, where the symbol m_e refers to the electron rest mass (9.1094×10^{-31} kg), and with n being taken as 1. Then applying the relation

$$\frac{E_{electron}}{E_{hole}} = \frac{m^*_{hole}}{m^*_{electron}} \tag{11}$$

we were easily able to solve for the effective mass of the hole, m^*_{hole}, light or heavy, respectively. When numerical values are used in place of the symbols in the equations above, the resulting values for the effective mass of the heavy-hole was $0.80m_e$, and for the light-hole was $0.24m_e$, as applied within the 93 Å well. These are in good comparison with values tabulated in the literature.

Conclusion:

In conclusion, it can be seen that the transition energies track linearly with the inverse square of well width, as predicted by the quantum mechanical equation of the infinite square well. Additionally, it can be seen that the technique of photoluminescence is a valuable tool in tracking the transition energies of a quantum well sample. It can also be seen that this approximation begins to fail at narrower well widths, at which point quantum tunneling becomes more prevalent. It can also be seen that the relationship between energy and temperature as predicted for GaAs is also applicable for the quantum well transitions, allowing us to predict their T = 0 K energy states, and the effective masses of the holes. Additionally, the temperature independence of the quantum confinement energies was verified. Studies of the temperature dependence of the photoluminescence spectra of various materials can now be undertaken with confidence knowing that precise and accurate results can be obtained using the spectroscopy laboratory in the WIU Physics Department.

Acknowledgements:

I'd like to take this time to thank Laurie A. Pichla and Michael C. Baxa for their assistance in collecting the raw data for this experiment.

I would also like to graciously thank my experimental spectroscopy and solid-state theory advisor Professor Mark S. Boley. Without his dedication to physics and higher education as well as his willingness to grant undergraduates the opportunity to perform laboratory research none of this work would have been possible. I would also like to thank Dr. Toni Sauncy for originally involving and getting me interested in the field of optical spectroscopy at WIU.

Finally I'd like to thank my parents Robert and Pamela Johnson for their moral and financial support as well as Alyssa Arends for her contributions to my mental and emotional well being.

References:

1. Liboff, Richard L., Introductory Quantum Mechanics, 3rd Edition, June 1997

2. Omar, M. Ali, Elementary Solid State Physics: Principles and Applications, 1975.

3. Kittel, Charles, Introduction to Solid State Physics, 7th Edition, July 1995

4. Boley, Mark, Optical Processes in Semiconductor Heterostructors, Ph.D. Thesis, August 1993

$E_{(T@0K)}$ (eV)	Hole	Well-Width
1.68	Light	47
1.62	Heavy	47
1.66	Light	70
1.60	Heavy	70
1.59	Light	93
1.57	Heavy	93
1.56	Heavy	117
1.55	Heavy	140

Table 1.

This table shows the predicted energy values for the light-hole and heavy-hole recombinations observed for each well width at absolute zero (T=0K).

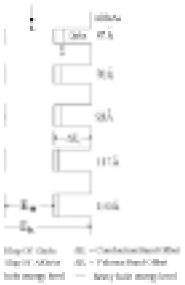

Figure1: Schematic of Multiple Quantum Well Sample

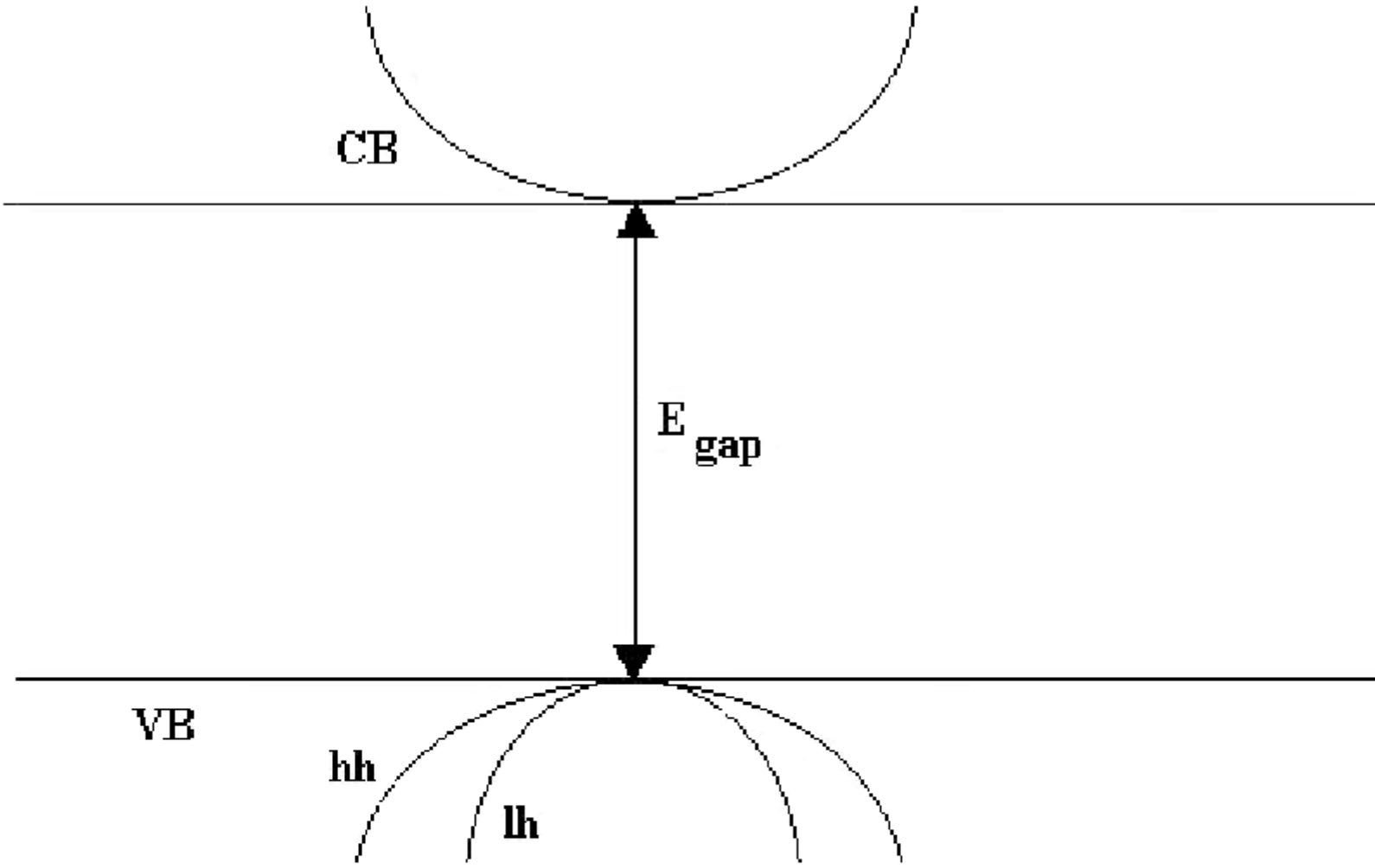

GaAs/AlGaAs III-V Semiconductor

CB-Conduction Band where the electrons move
VB-Valence Band where the holes move
hh-heavy holes lh-light holes

Figure 2: GaAs Direct Bandgap Transition Diagram

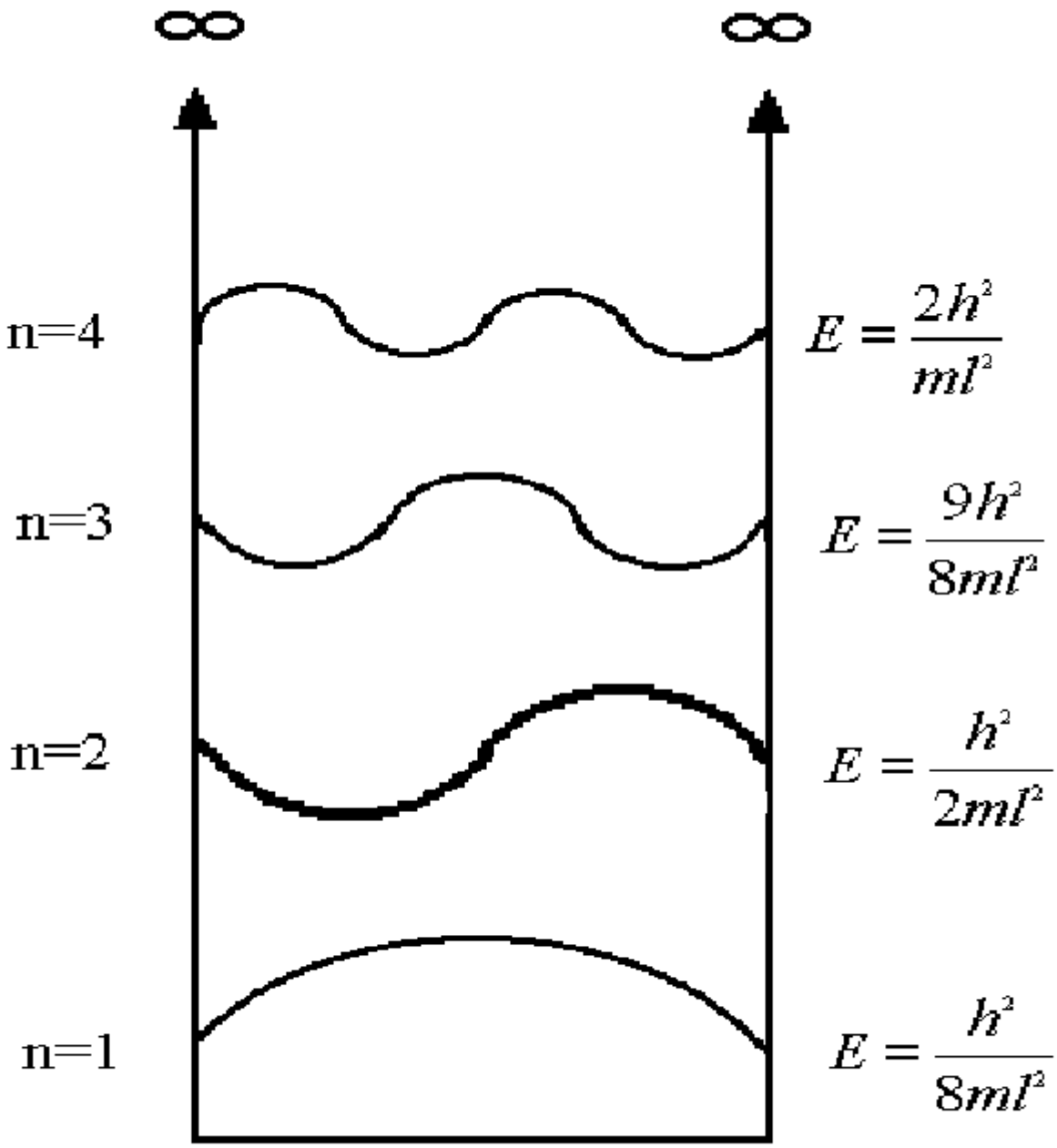

Figure 3: Infinite Square Well Energies and Quantum Numbers

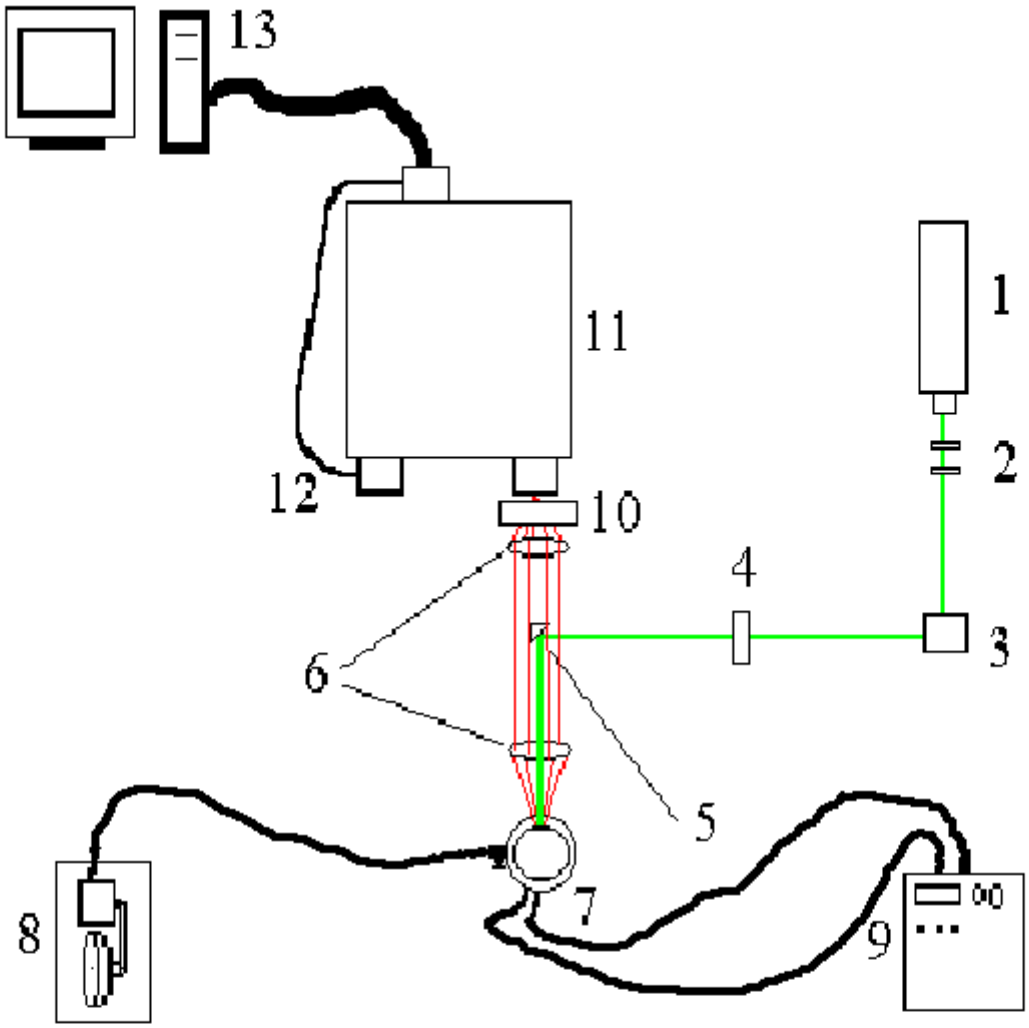

1 Argon Ion Laser (4880Å)
2 Neutral Density Filters
3 Mirrors
4 4880Å Line filter
5 Prism Mirror
6 Focusing Lenses
7 Cold Head/Sample Mount
8 Vacuum/Roughing Pump
9 Helium Refrigerator
10 Super Notch Filter
11 Spectrometer
12 GaAs PMT
13 Computer/Labview

Scattered Light
4880Å Beam

Figure 4: Schematic of Experimental Apparatus

MQW Spectrum T@ 21K

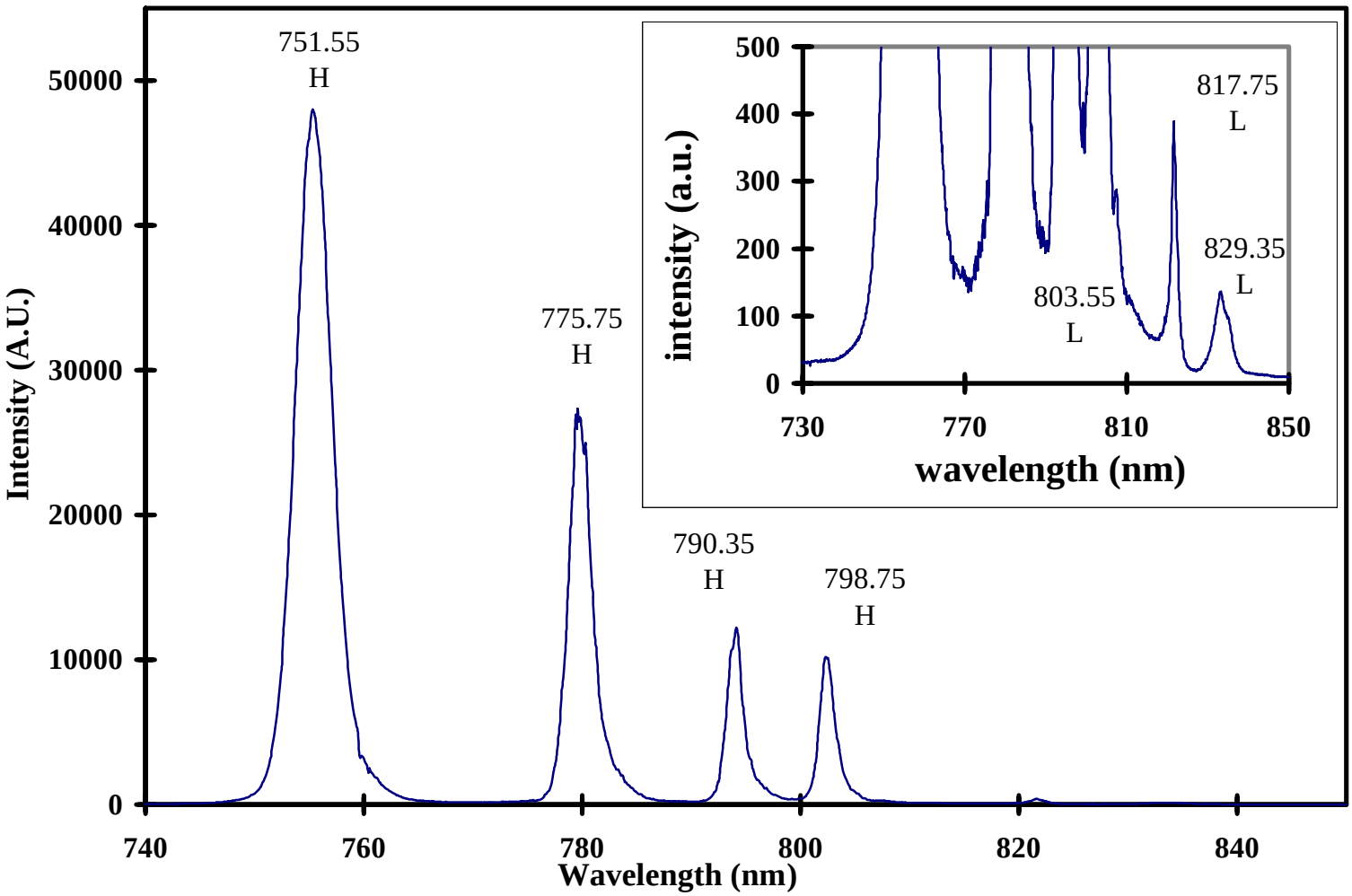

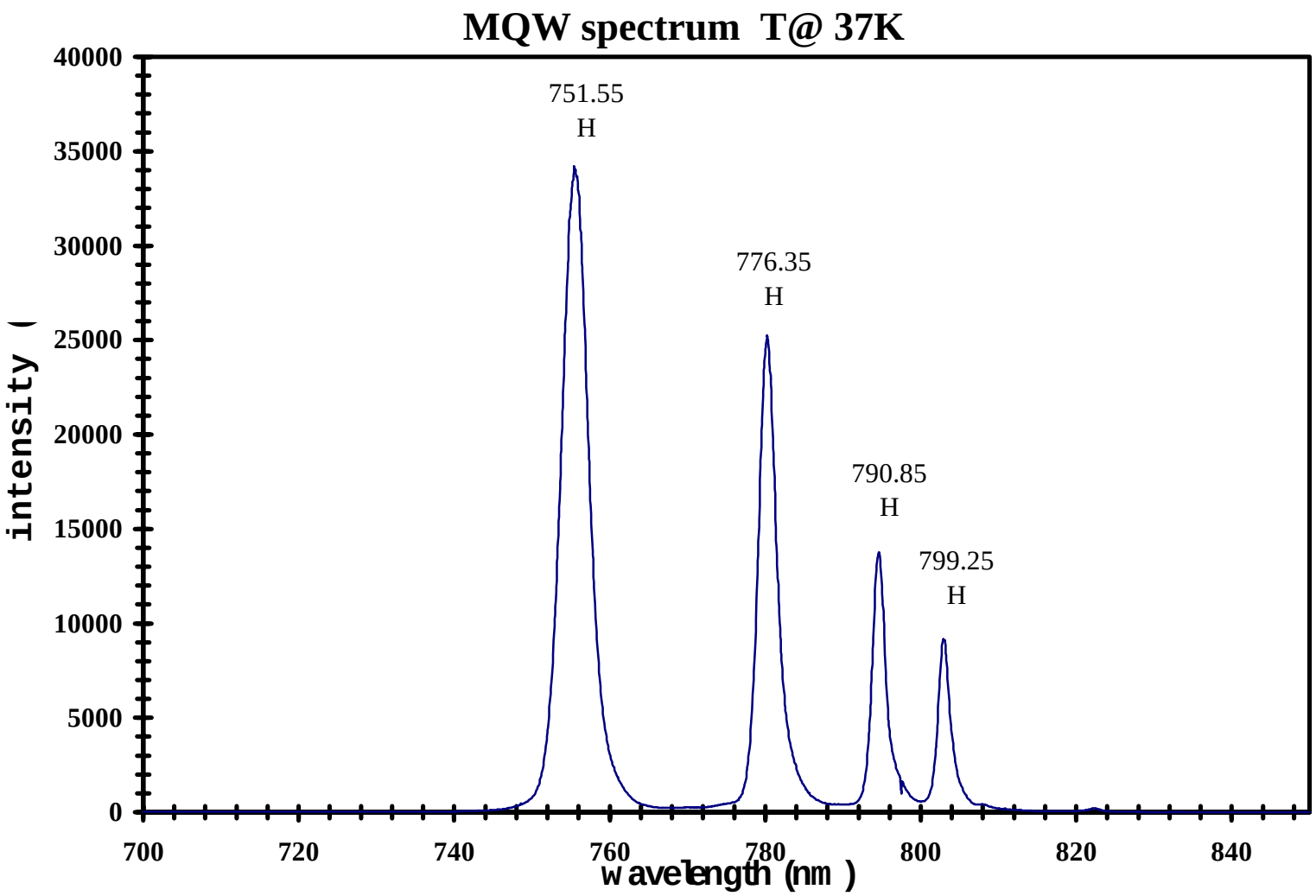
MQW spectrum T@ 37K
751.55
H
776.35
H
790.85
H
799.25
H
intensity (
wavelength (nm)
40000
35000
30000
25000
20000
15000
10000
5000
0
700
720
740
760
780
800
820
840

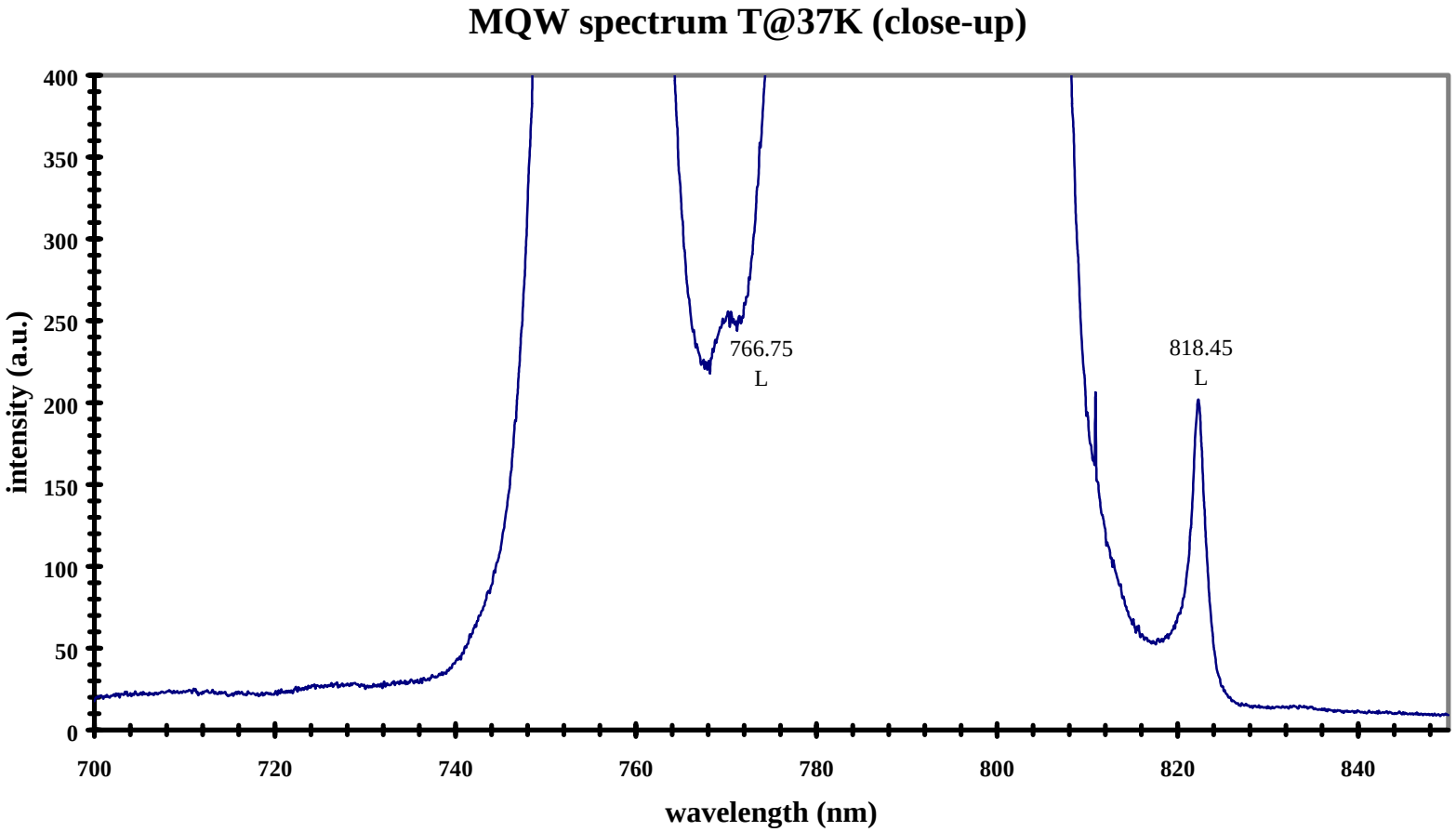
MQW spectrum T@37K (close-up)
intensity (a.u.)
400
350
300
250
200
150
100
50
0
700
720
740
760
780
800
820
840
wavelength (nm)
766.75
L
818.45
L

MQW spectrum T @ 53K

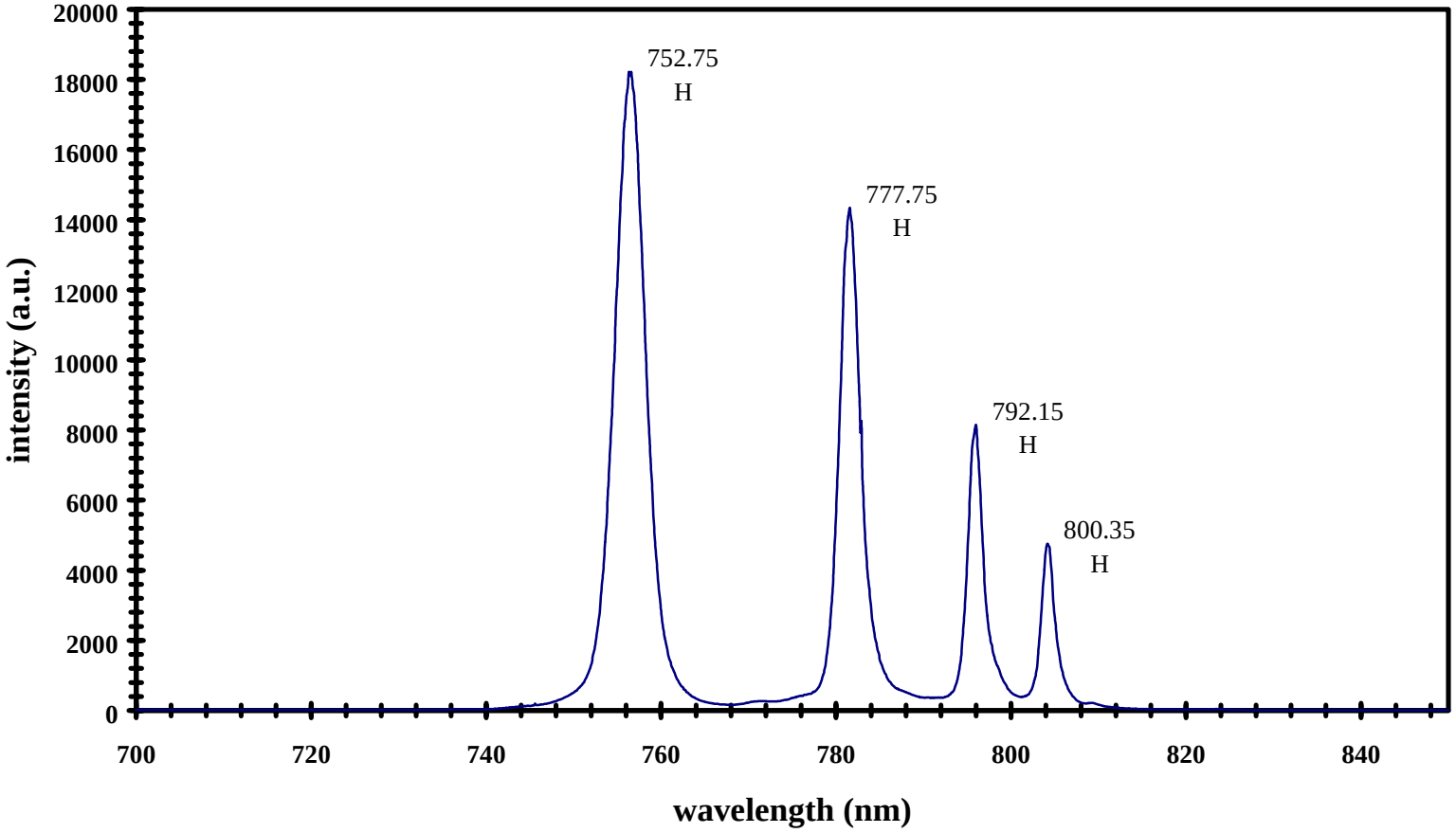

MQW spectrum T @ 53K (close-up)

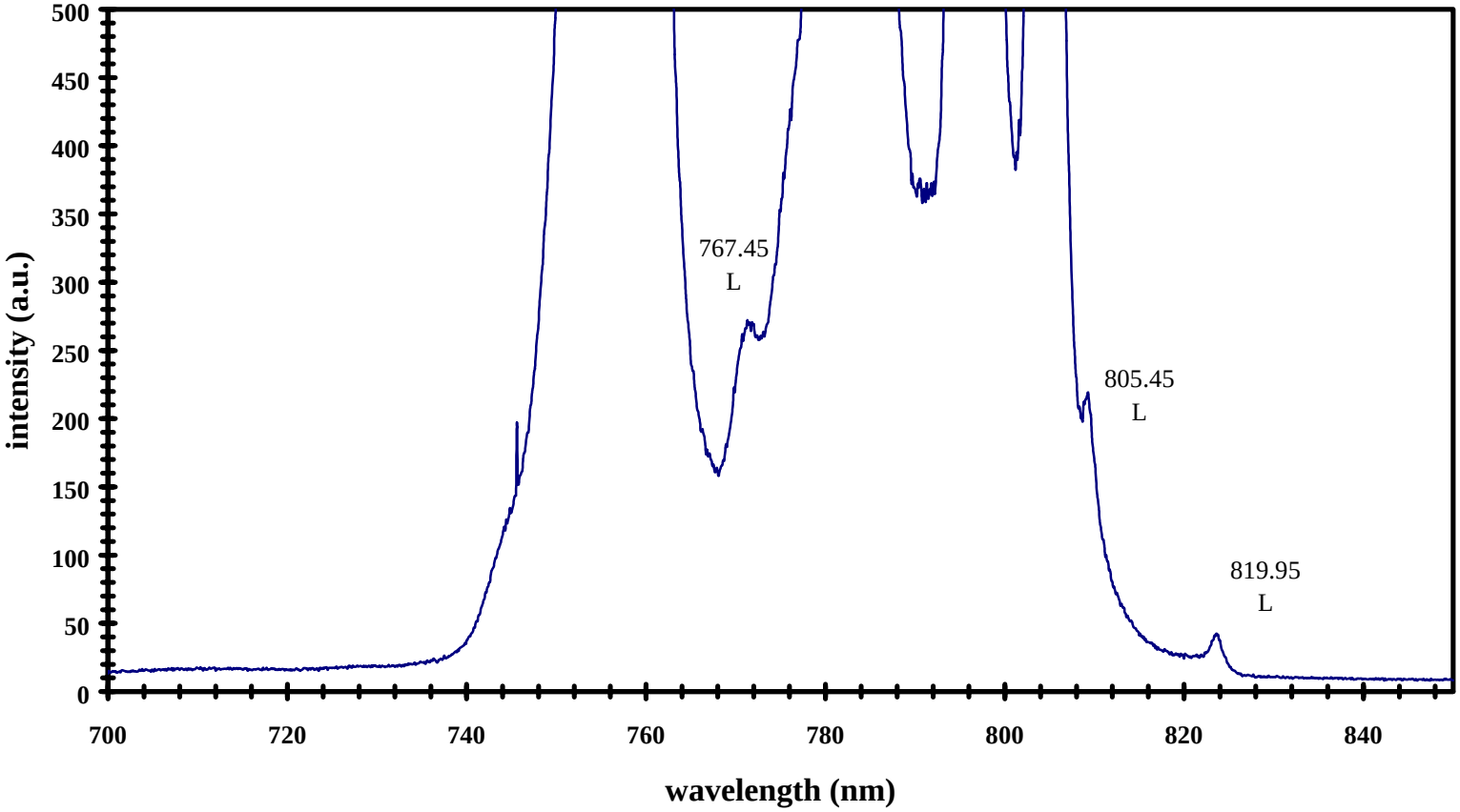

MQW spectrum T@75K

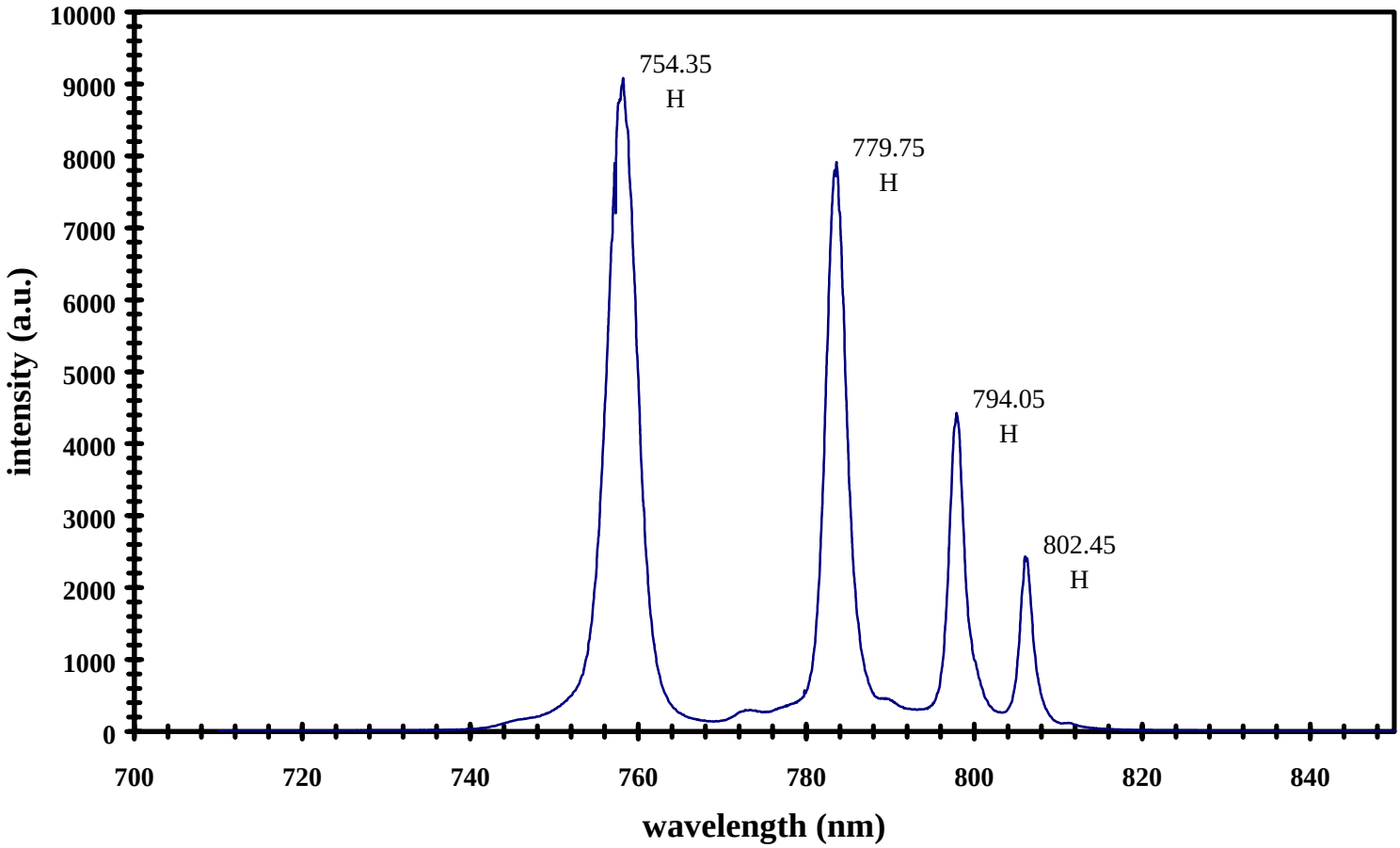

MQW spectrum T@75K (close-up)

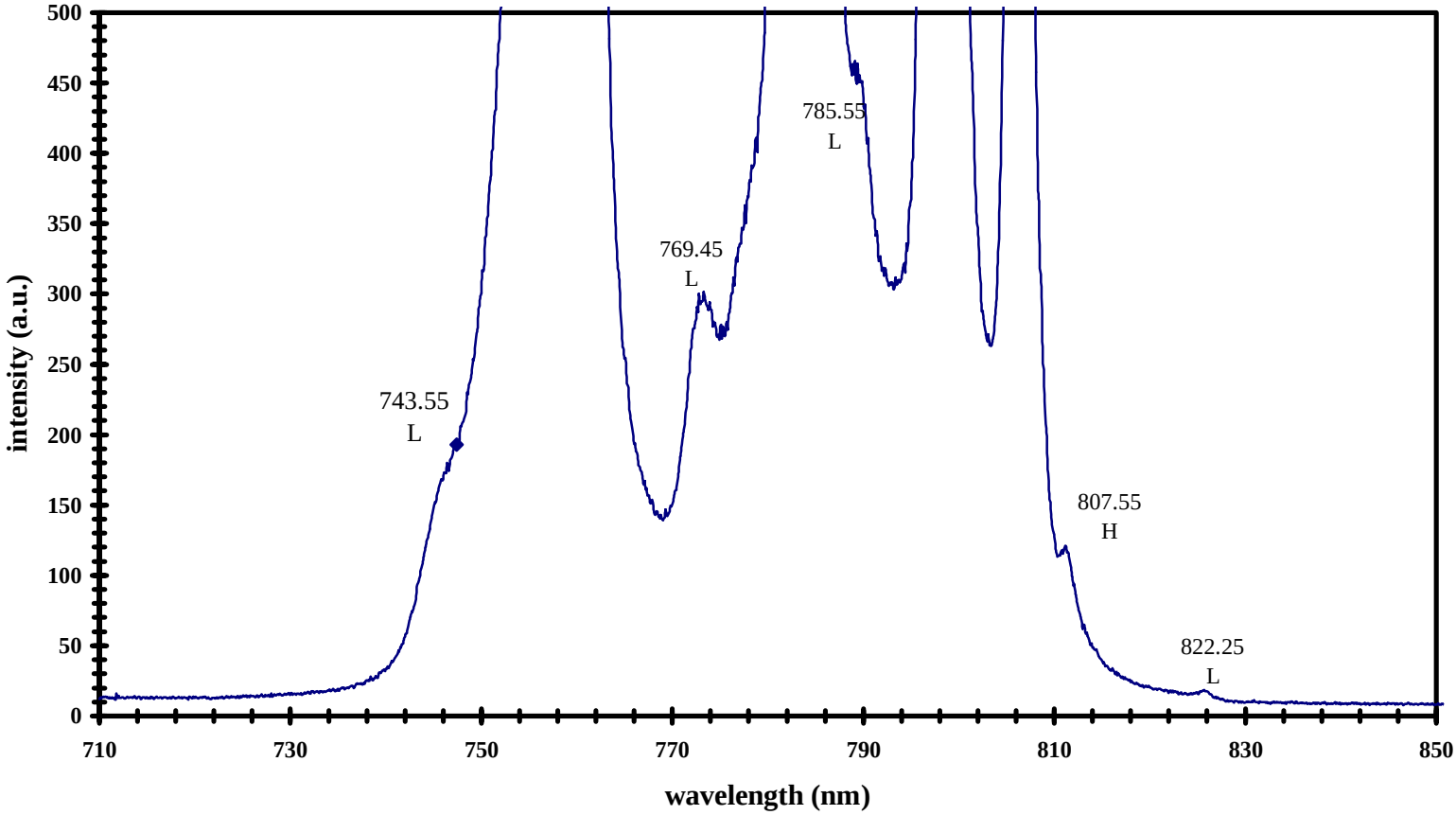

MQW spectrum T@100K

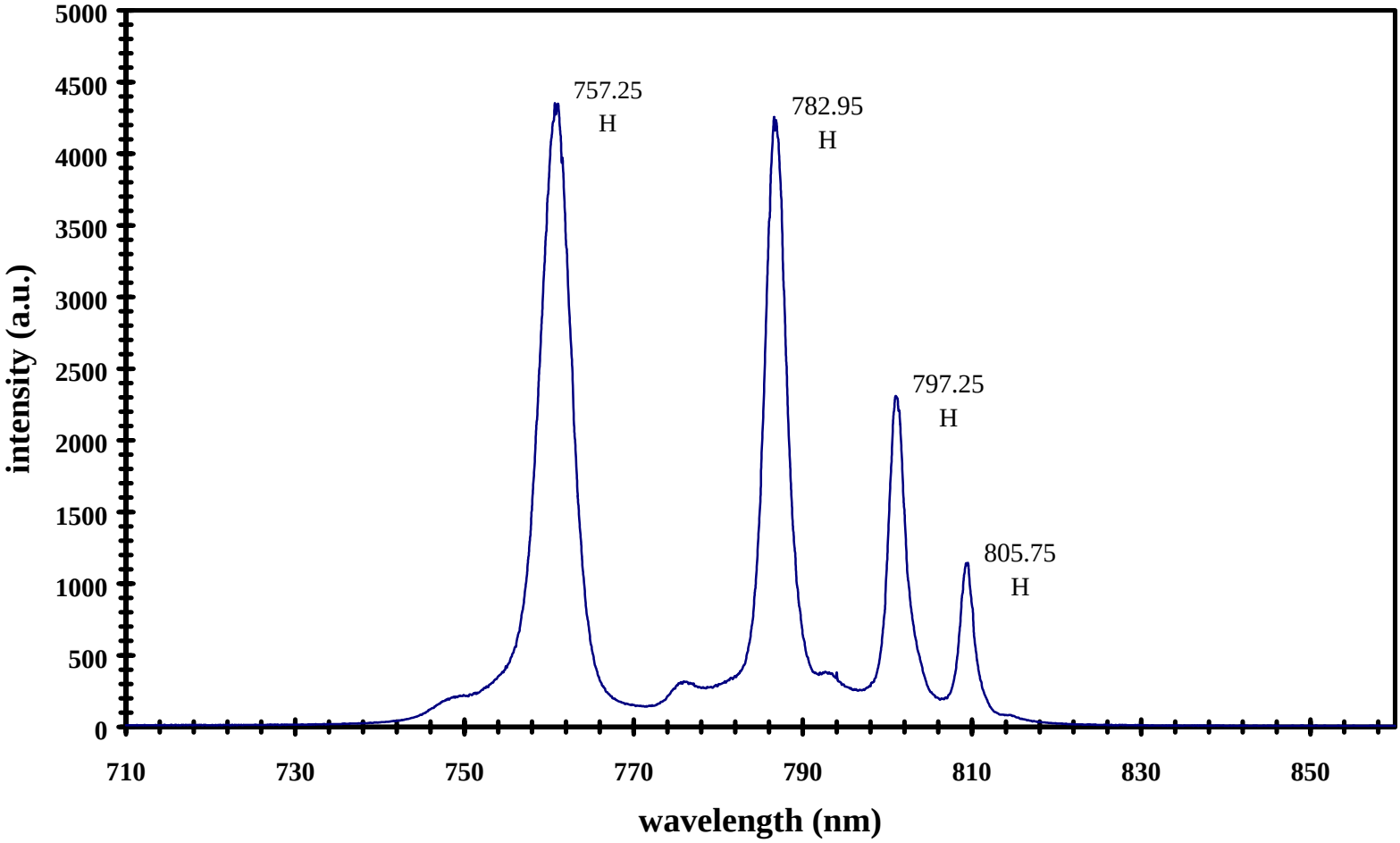

MQW spectrum T@100K (close-up)

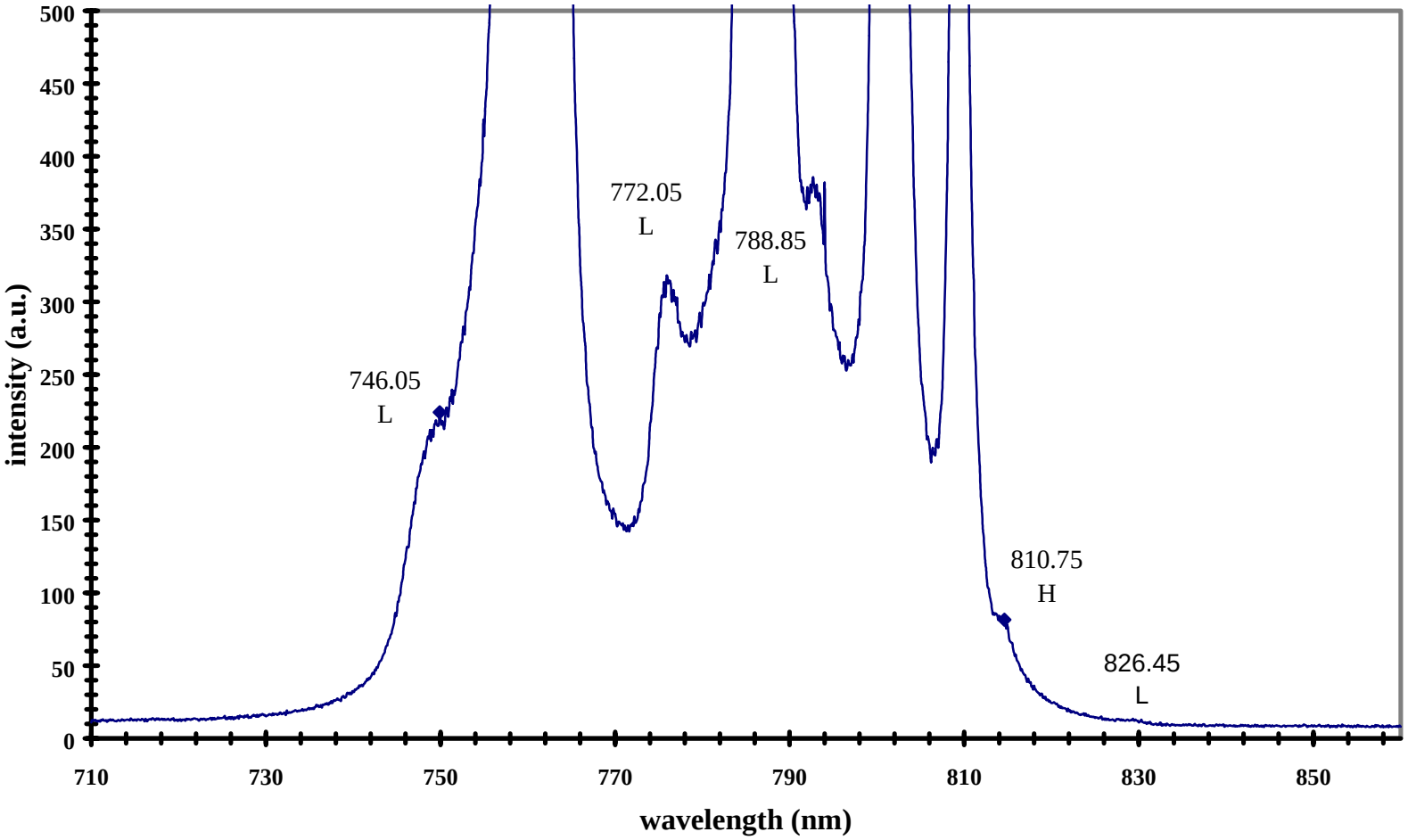

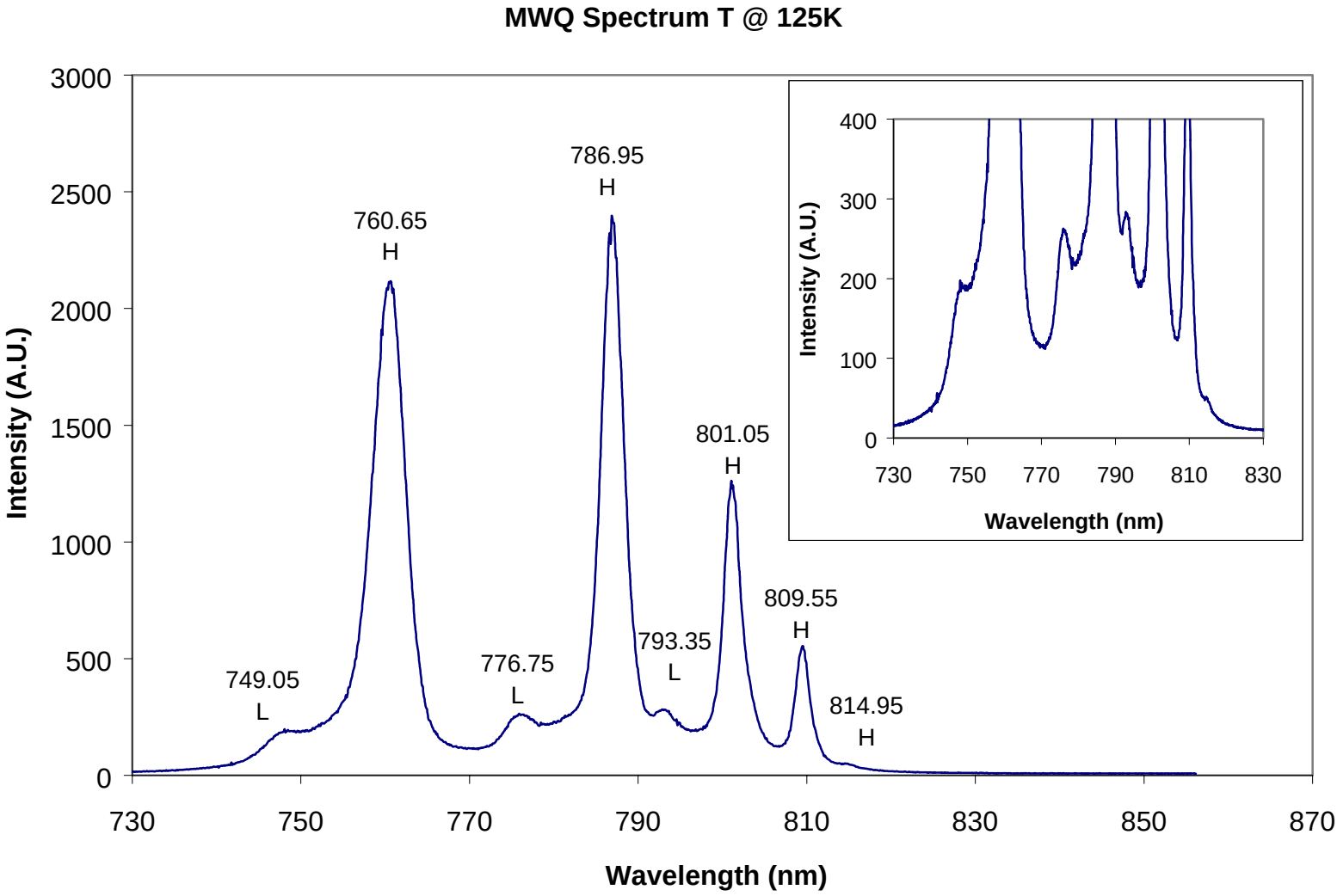
MWQ Spectrum T @ 125K
Intensity (A.U.)
Wavelength (nm)
760.65
H
786.95
H
801.05
H
809.55
H
749.05
L
776.75
L
793.35
L
814.95
H
Intensity (A.U.)
Wavelength (nm)

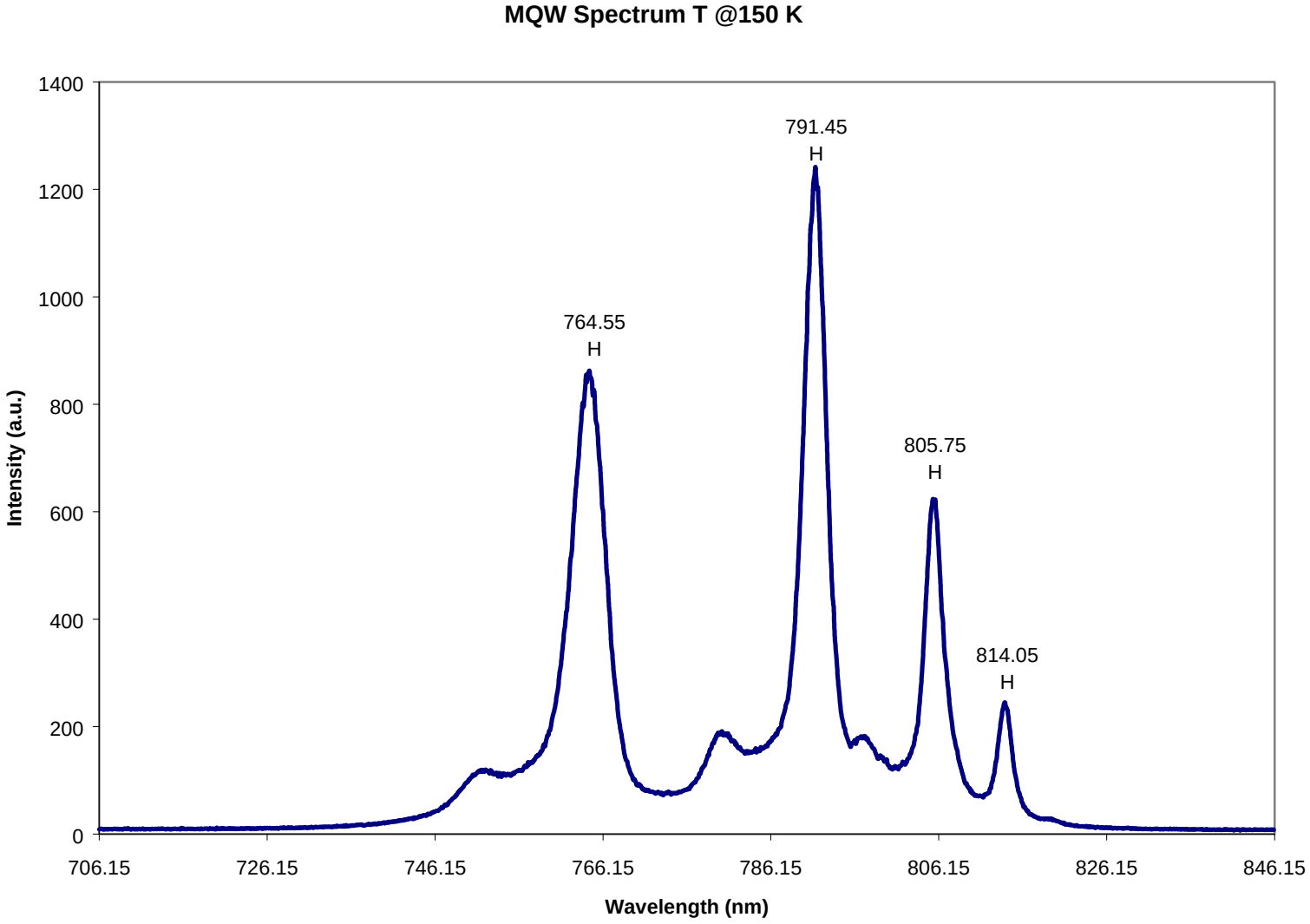
MQW Spectrum T @150 K
1400
1200
1000
800
600
400
200
0
Intensity (a.u.)
764.55
H
791.45
H
805.75
H
814.05
H
706.15
726.15
746.15
766.15
786.15
806.15
826.15
846.15
Wavelength (nm)

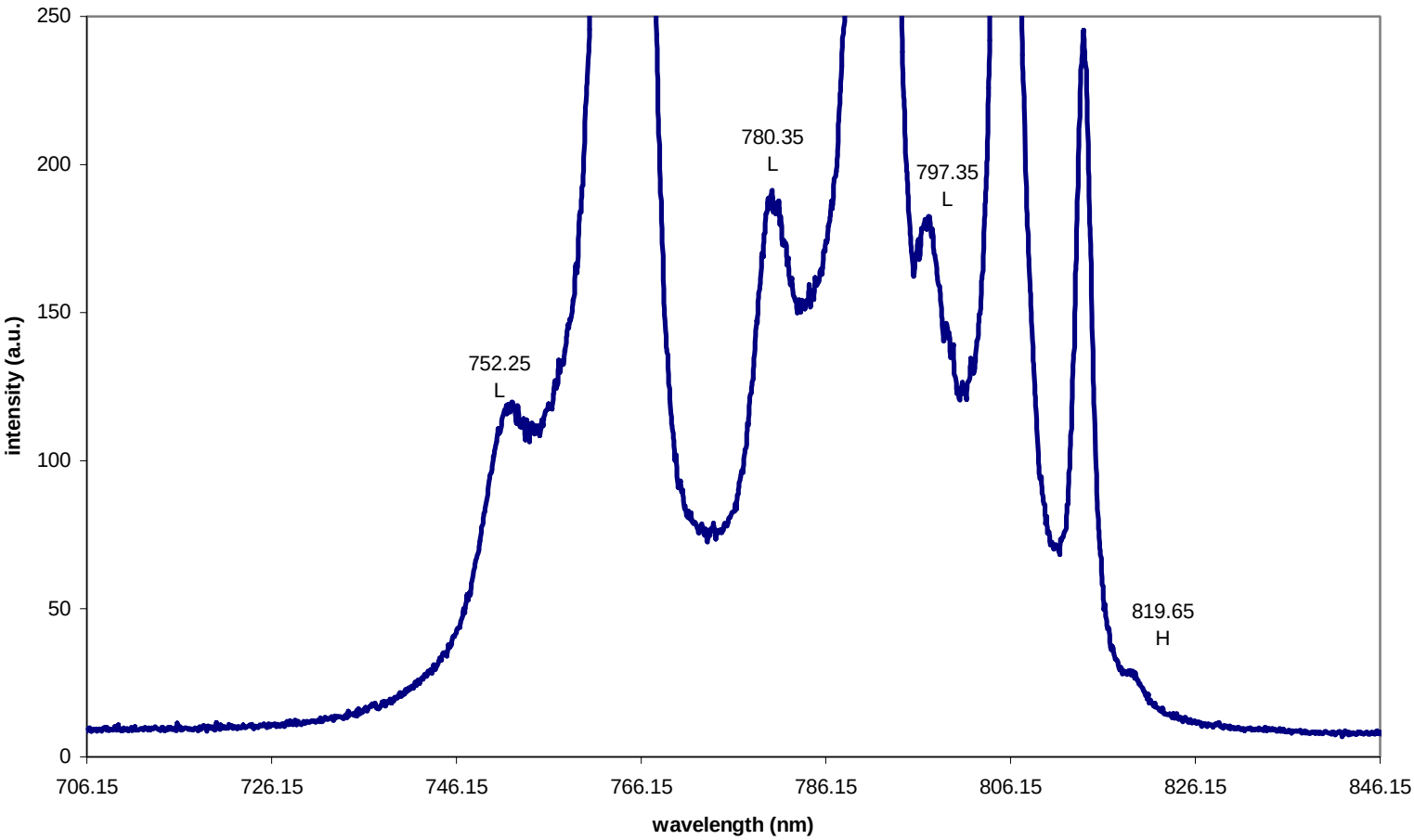
MQW spectrum T@150K (close up)
250
200
150
100
50
0
intensity (a.u.)
752.25
L
780.35
L
797.35
L
819.65
H
706.15
726.15
746.15
766.15
786.15
806.15
826.15
846.15
wavelength (nm)

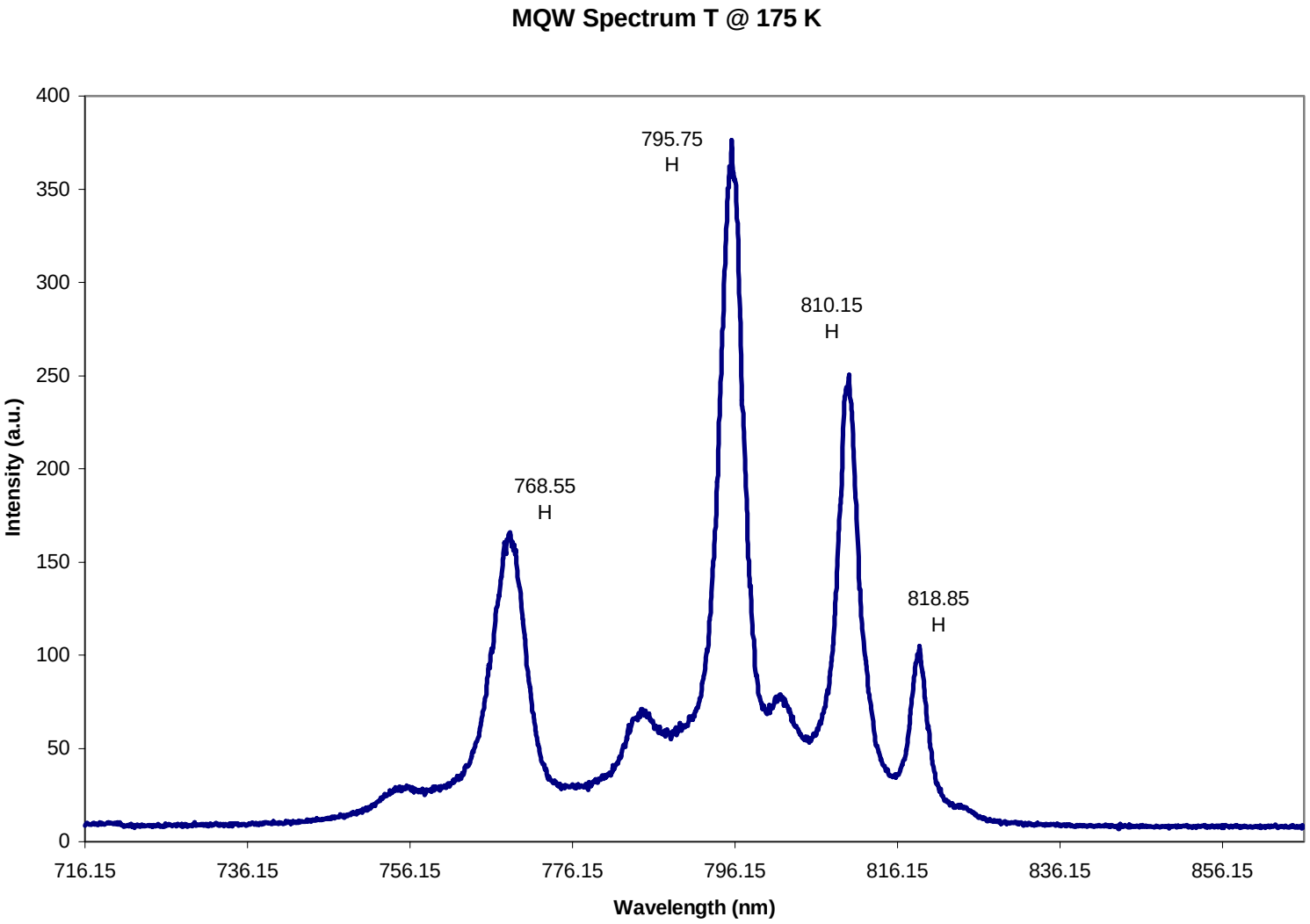
MQW Spectrum T @ 175 K
Intensity (a.u.)
400
350
300
250
200
150
100
50
0
795.75
H
810.15
H
768.55
H
818.85
H
716.15
736.15
756.15
776.15
796.15
816.15
836.15
856.15
Wavelength (nm)

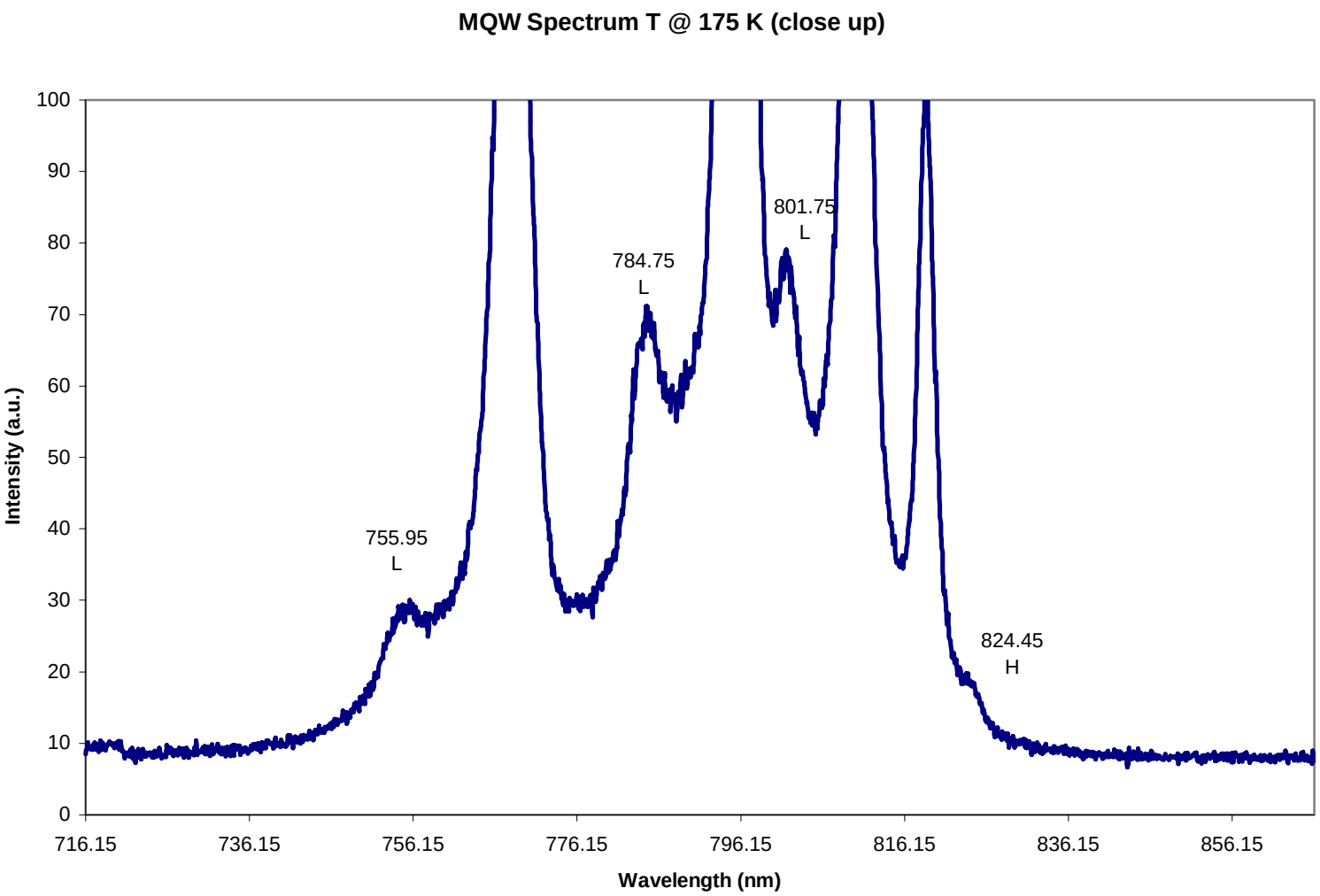
MQW Spectrum T @ 175 K (close up)
Intensity (a.u.)
100
90
80
70
60
50
40
30
20
10
0
716.15
736.15
756.15
776.15
796.15
816.15
836.15
856.15
Wavelength (nm)
755.95
L
784.75
L
801.75
L
824.45
H

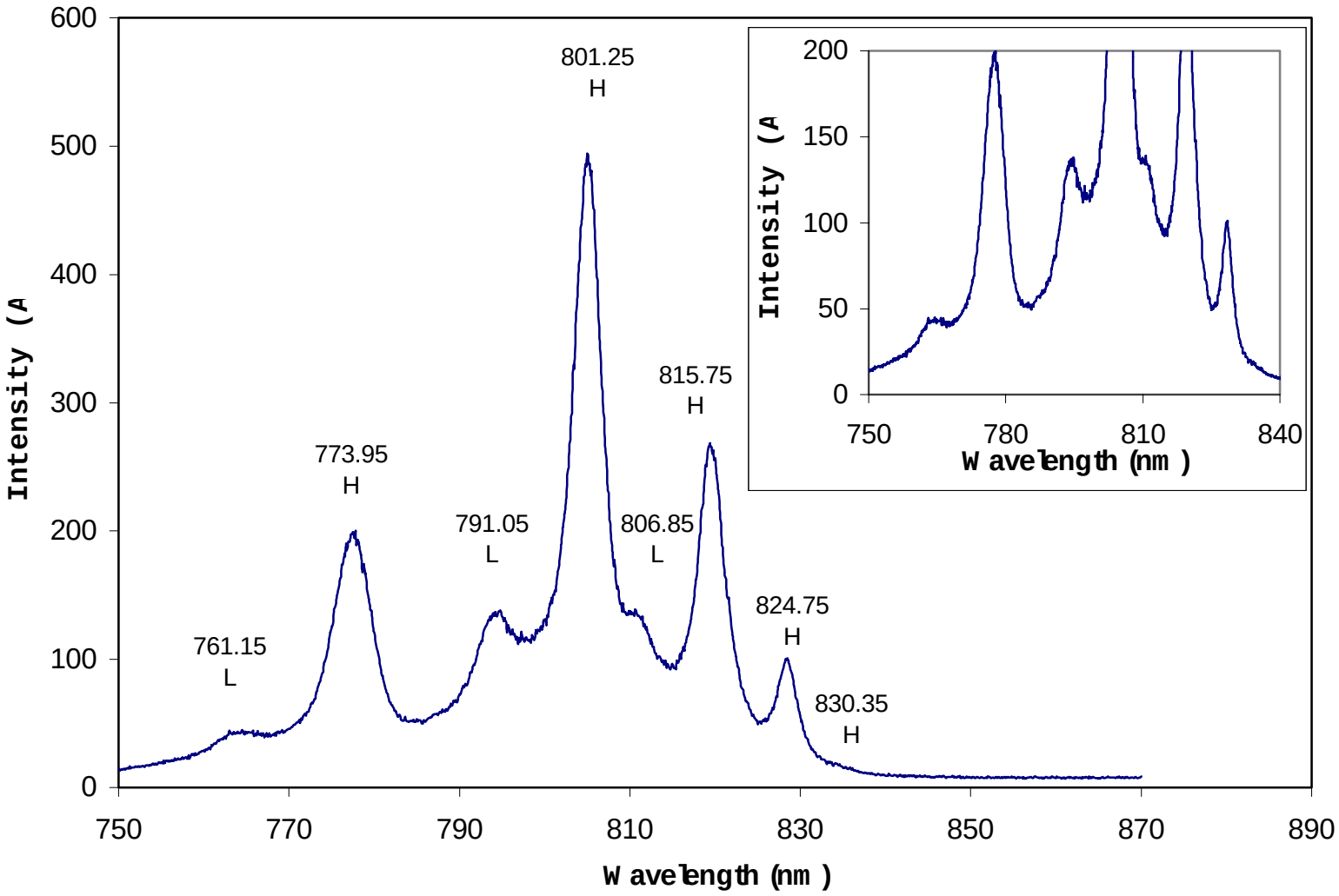
MQW Spectrum T@ 200K
Intensity (A
Wavelength (nm)
761.15
L
773.95
H
791.05
L
801.25
H
806.85
L
815.75
H
824.75
H
830.35
H
Intensity (A
Wavelength (nm)

MQW Spectrum T@ 220K

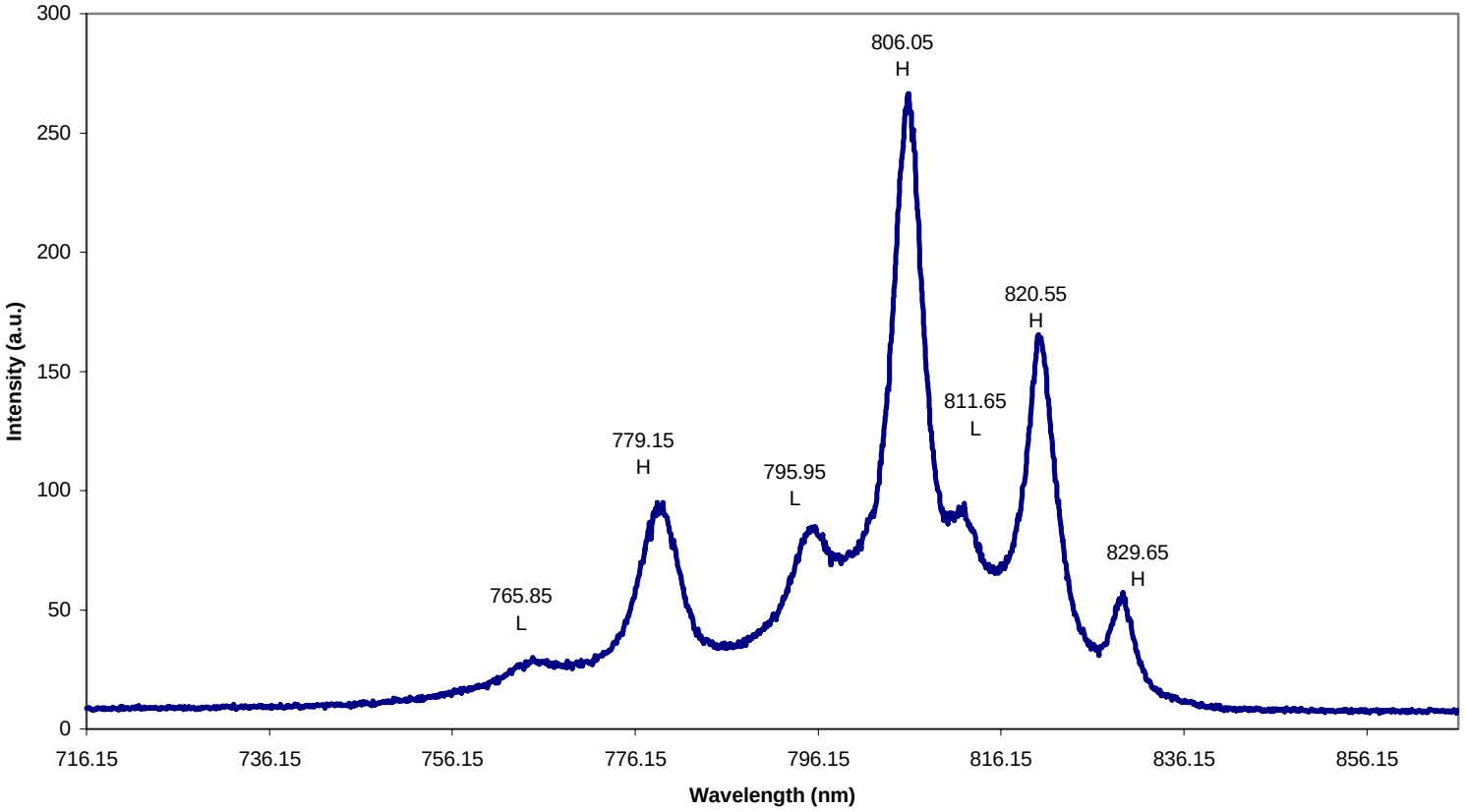

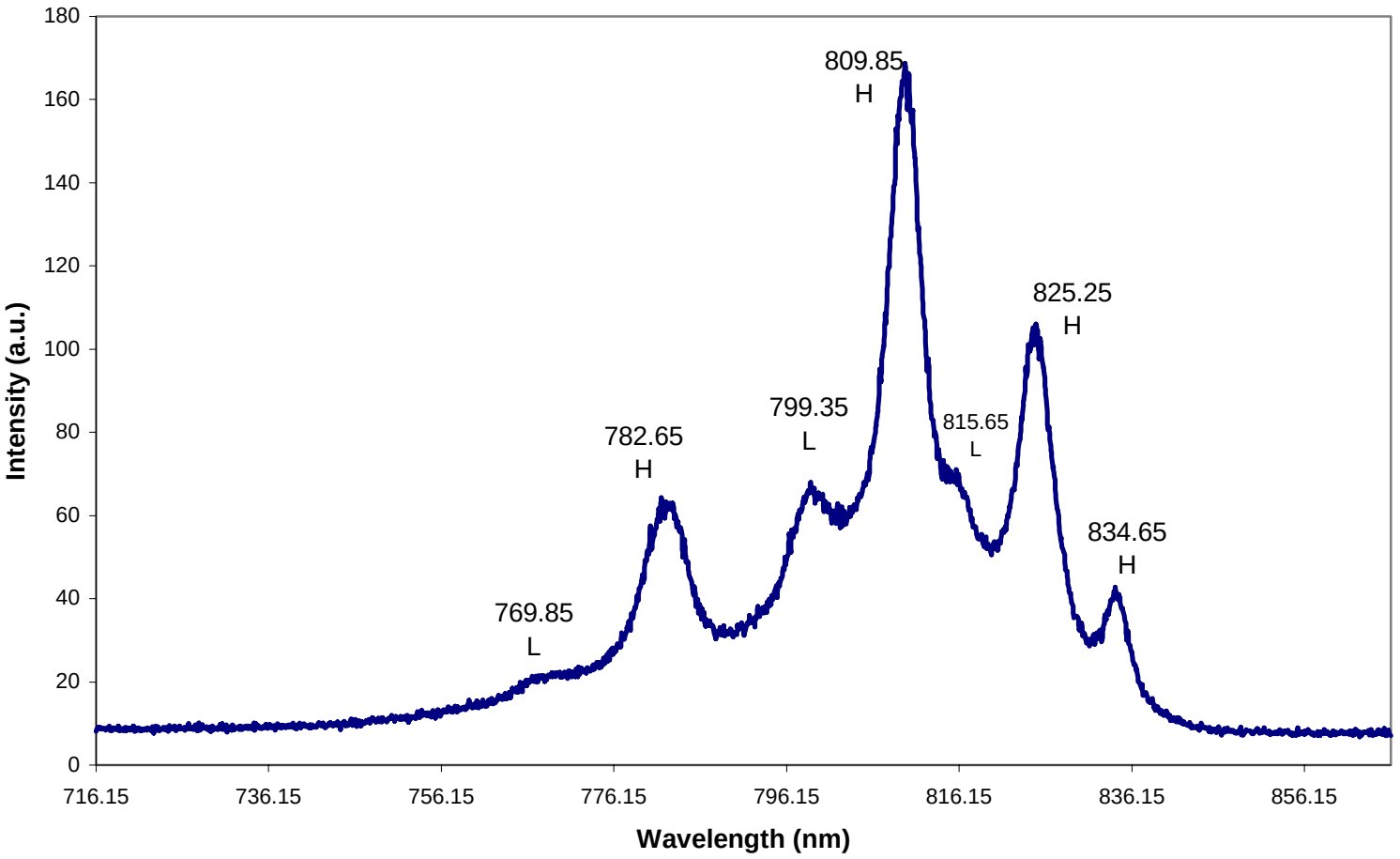
MQW Spectrum T @ 241 K
Intensity (a.u.)
180
160
140
120
100
80
60
40
20
0
716.15
736.15
756.15
776.15
796.15
816.15
836.15
856.15
Wavelength (nm)
769.85
L
782.65
H
799.35
L
809.85
H
815.65
L
825.25
H
834.65
H

MQW Spectrum T@ 270 K

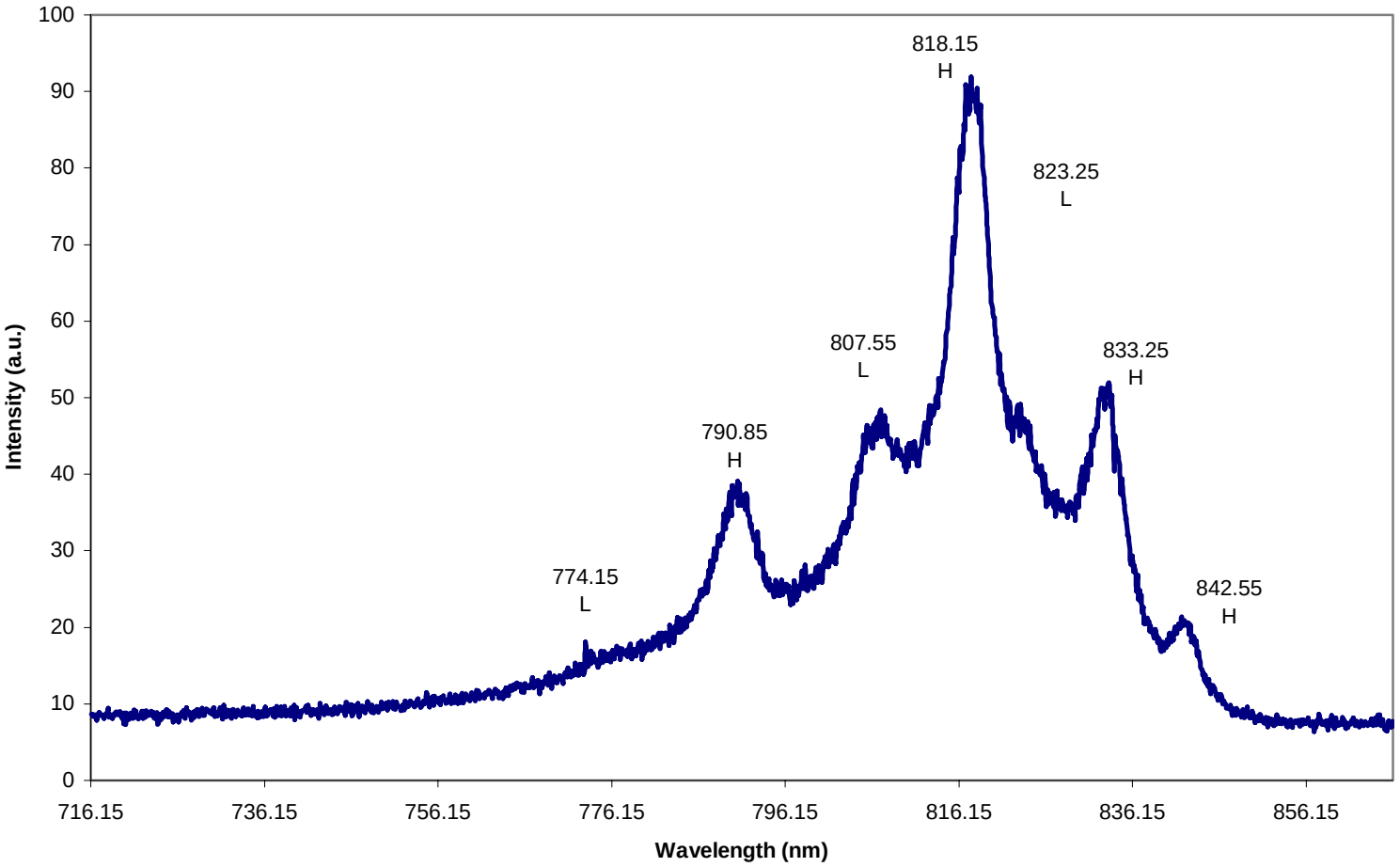

MQW Spectrum T@291 K

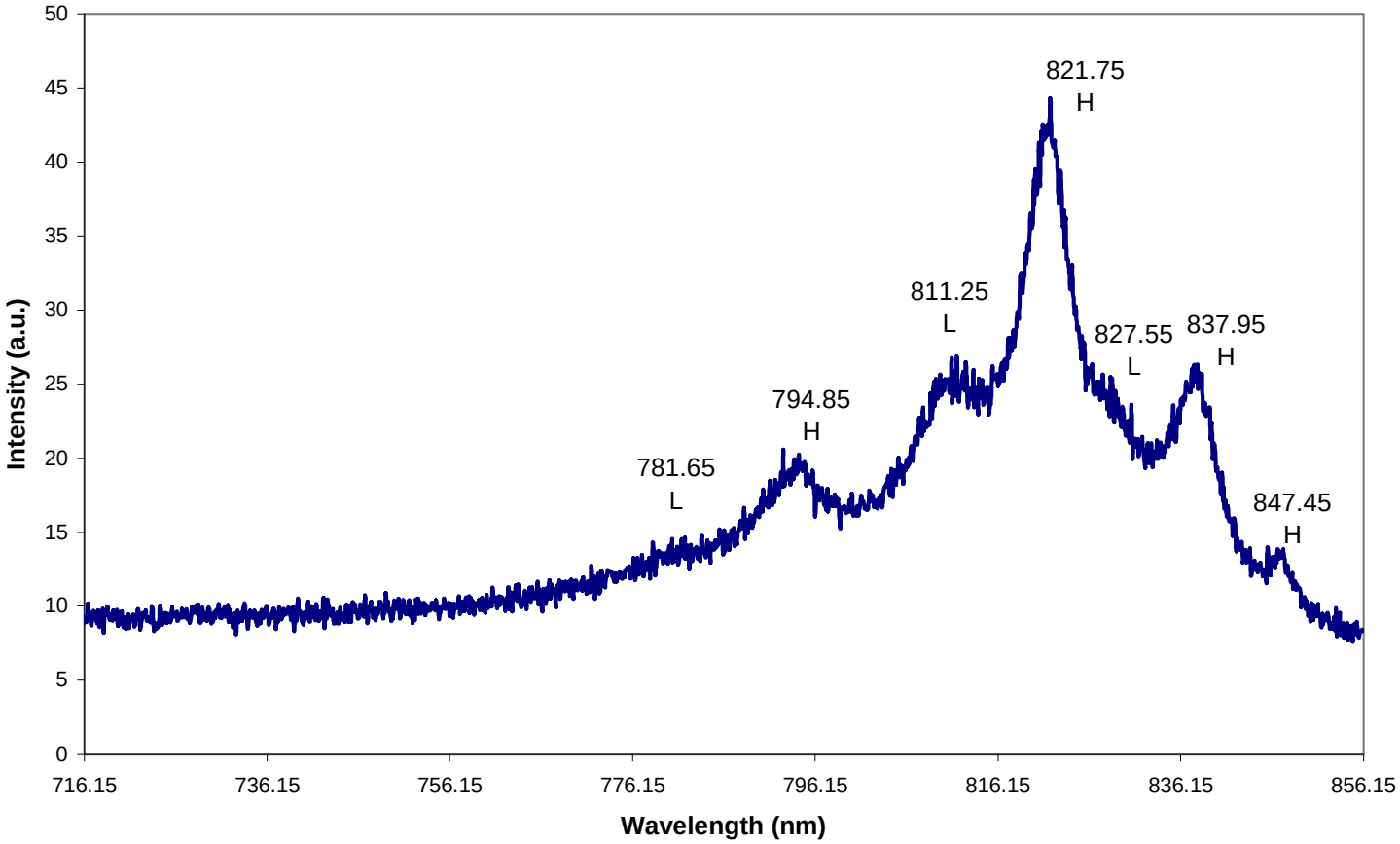

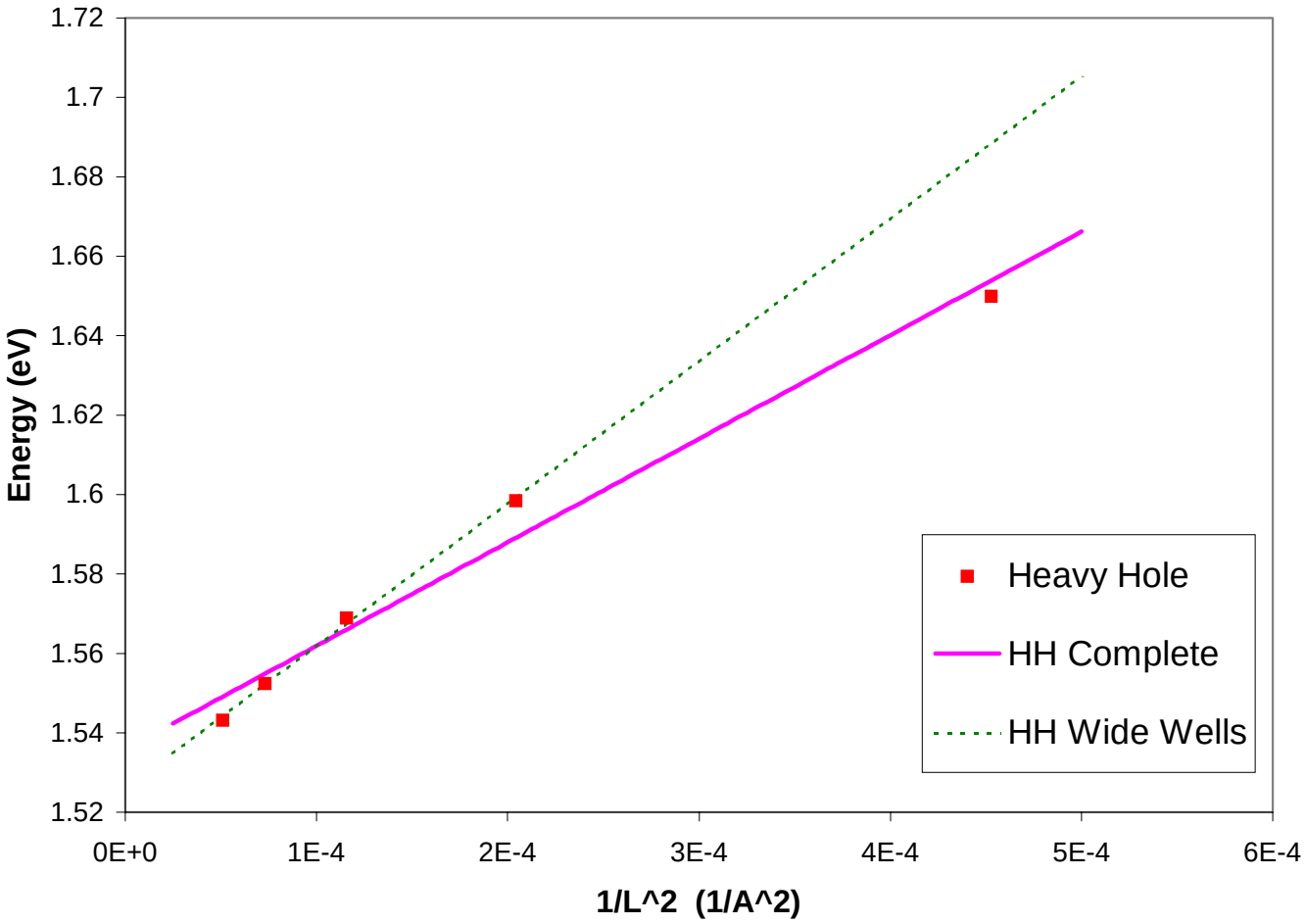
MQW E vs inv(1/L^2) T@21K heavy (47,70,93,117,140)
Energy (eV)
1.72
1.7
1.68
1.66
1.64
1.62
1.6
1.58
1.56
1.54
1.52
0E+0
1E-4
2E-4
3E-4
4E-4
5E-4
6E-4
1/L^2 (1/A^2)
Heavy Hole
HH Complete
HH Wide Wells

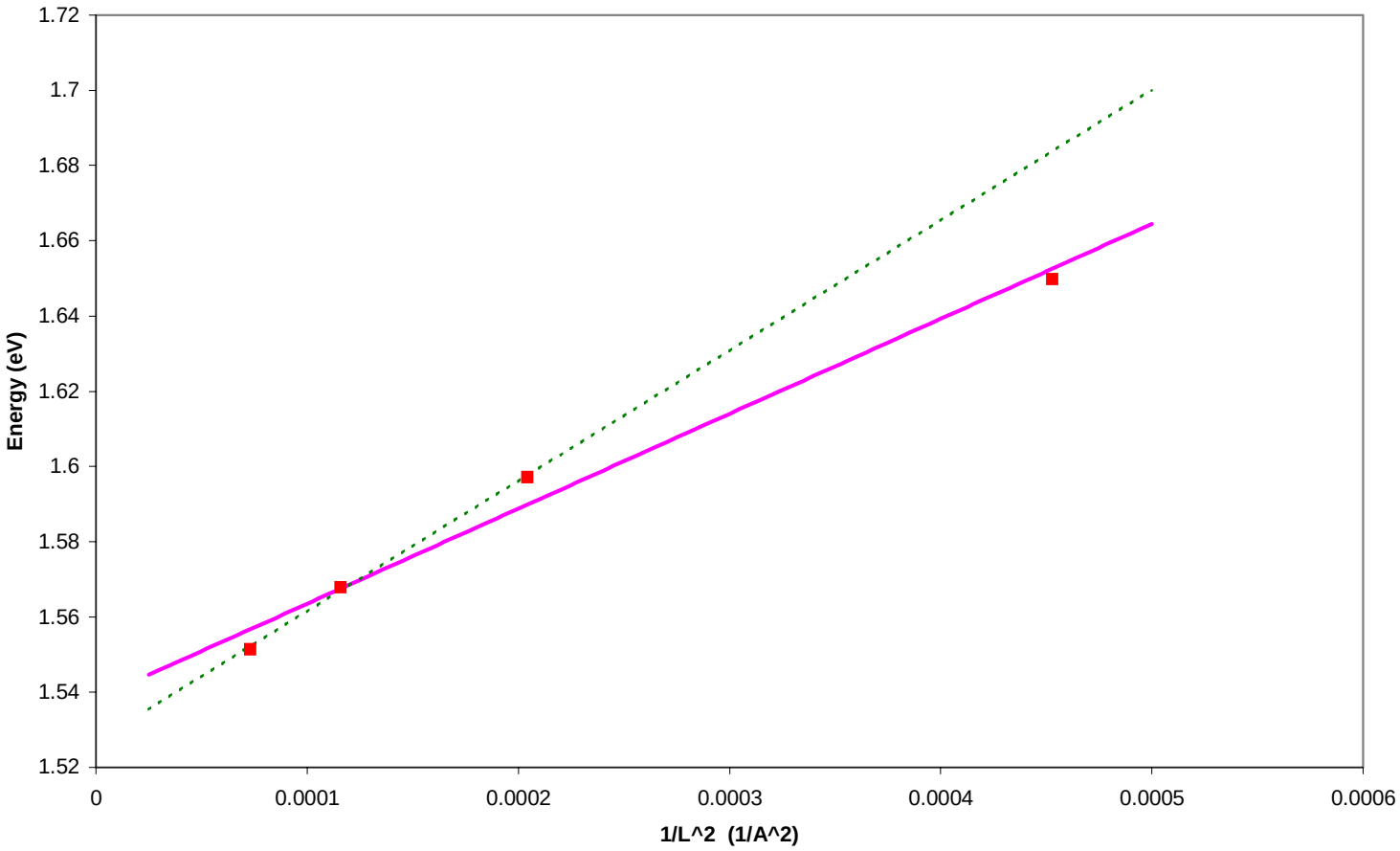
MQW E vs inv(1/L^2) T@37K heavy (47,70,93,117)
Energy (eV)
1.72
1.7
1.68
1.66
1.64
1.62
1.6
1.58
1.56
1.54
1.52
0
0.0001
0.0002
0.0003
0.0004
0.0005
0.0006
1/L^2 (1/A^2)

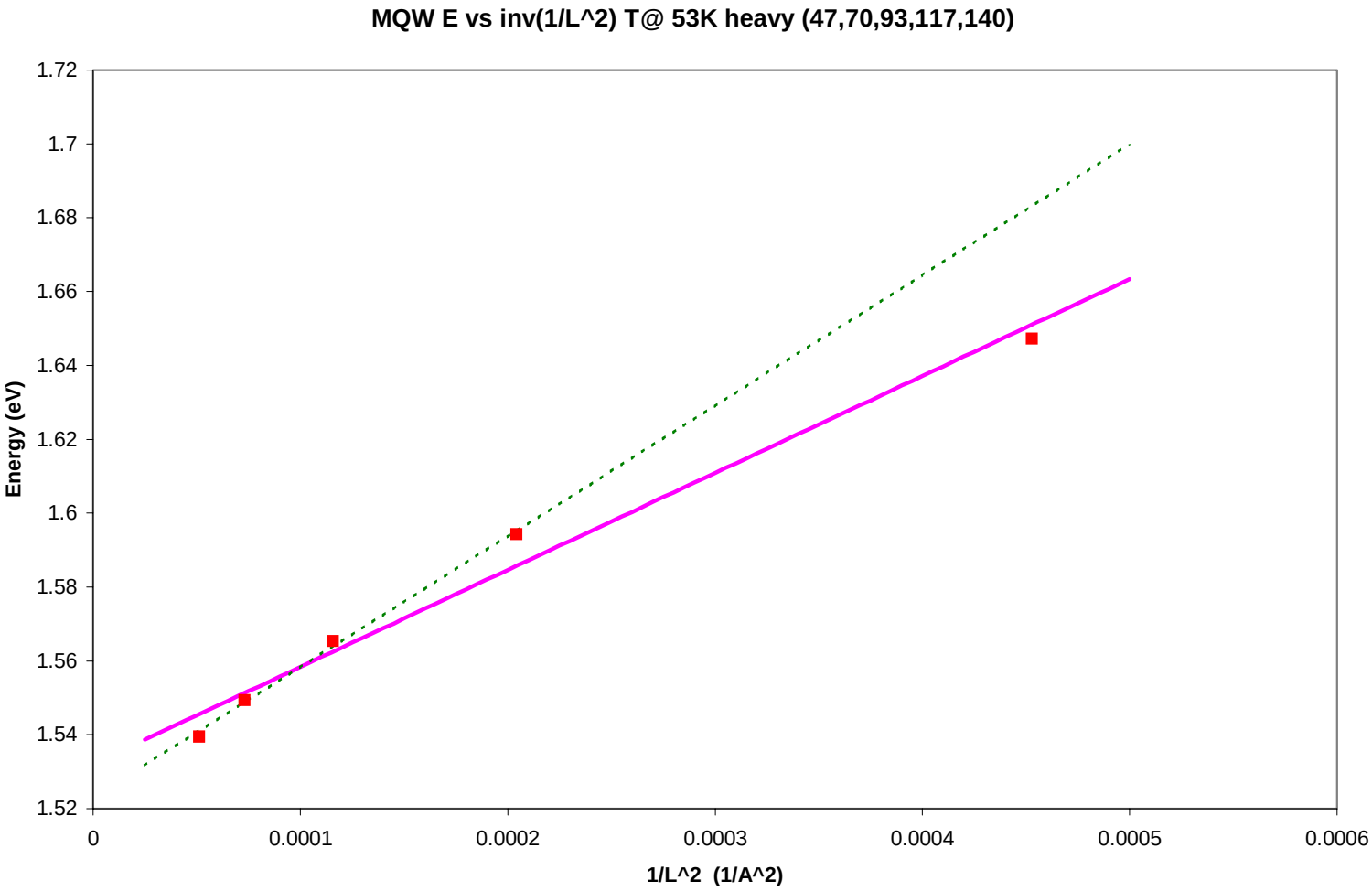
MQW E vs inv(1/L^2) T@ 53K heavy (47,70,93,117,140)
Energy (eV)
1.72
1.7
1.68
1.66
1.64
1.62
1.6
1.58
1.56
1.54
1.52
0
0.0001
0.0002
0.0003
0.0004
0.0005
0.0006
1/L^2 (1/A^2)

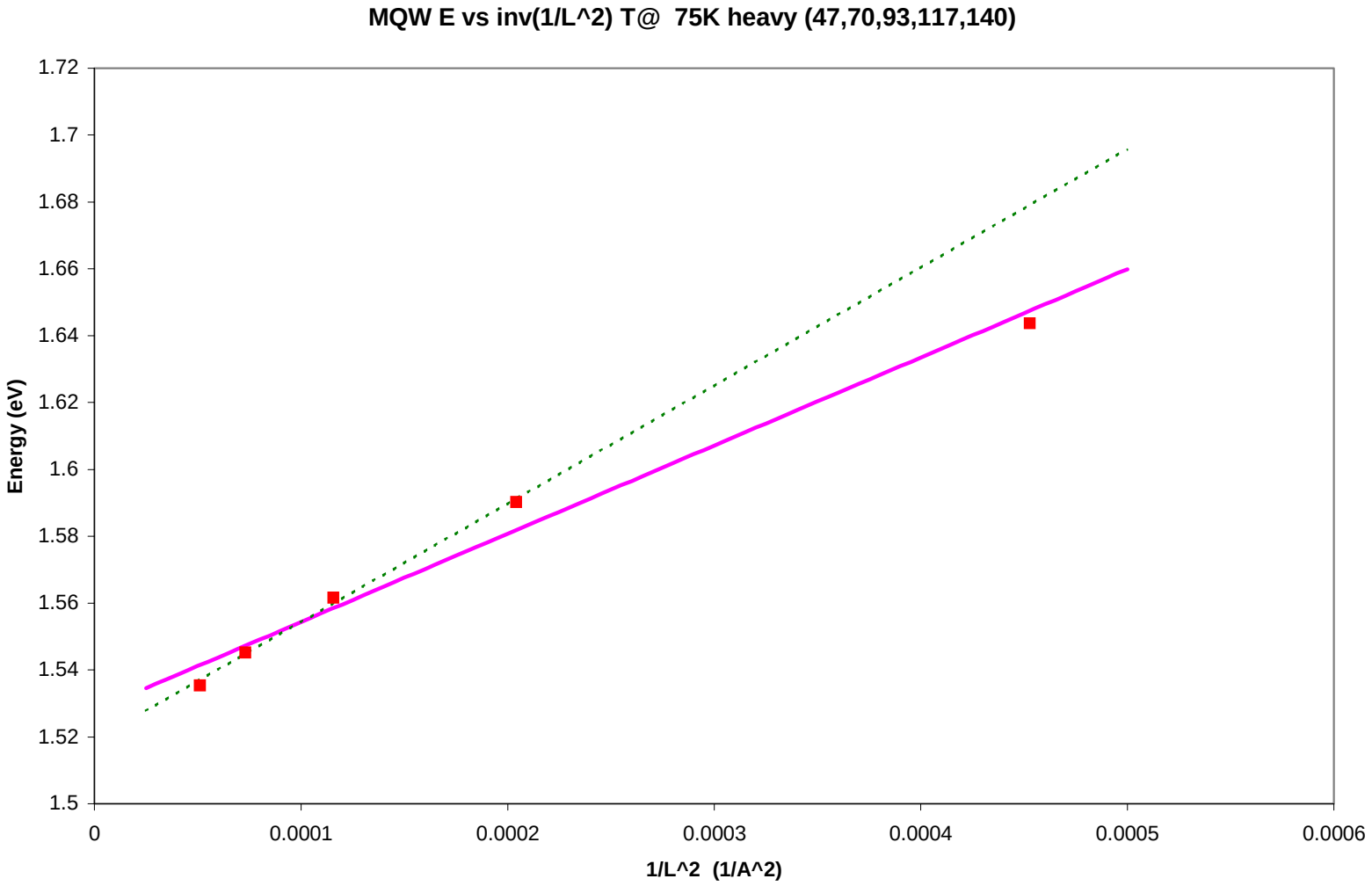
MQW E vs inv(1/L^2) T@ 75K heavy (47,70,93,117,140)
Energy (eV)
1.72
1.7
1.68
1.66
1.64
1.62
1.6
1.58
1.56
1.54
1.52
1.5
0
0.0001
0.0002
0.0003
0.0004
0.0005
0.0006
1/L^2 (1/A^2)

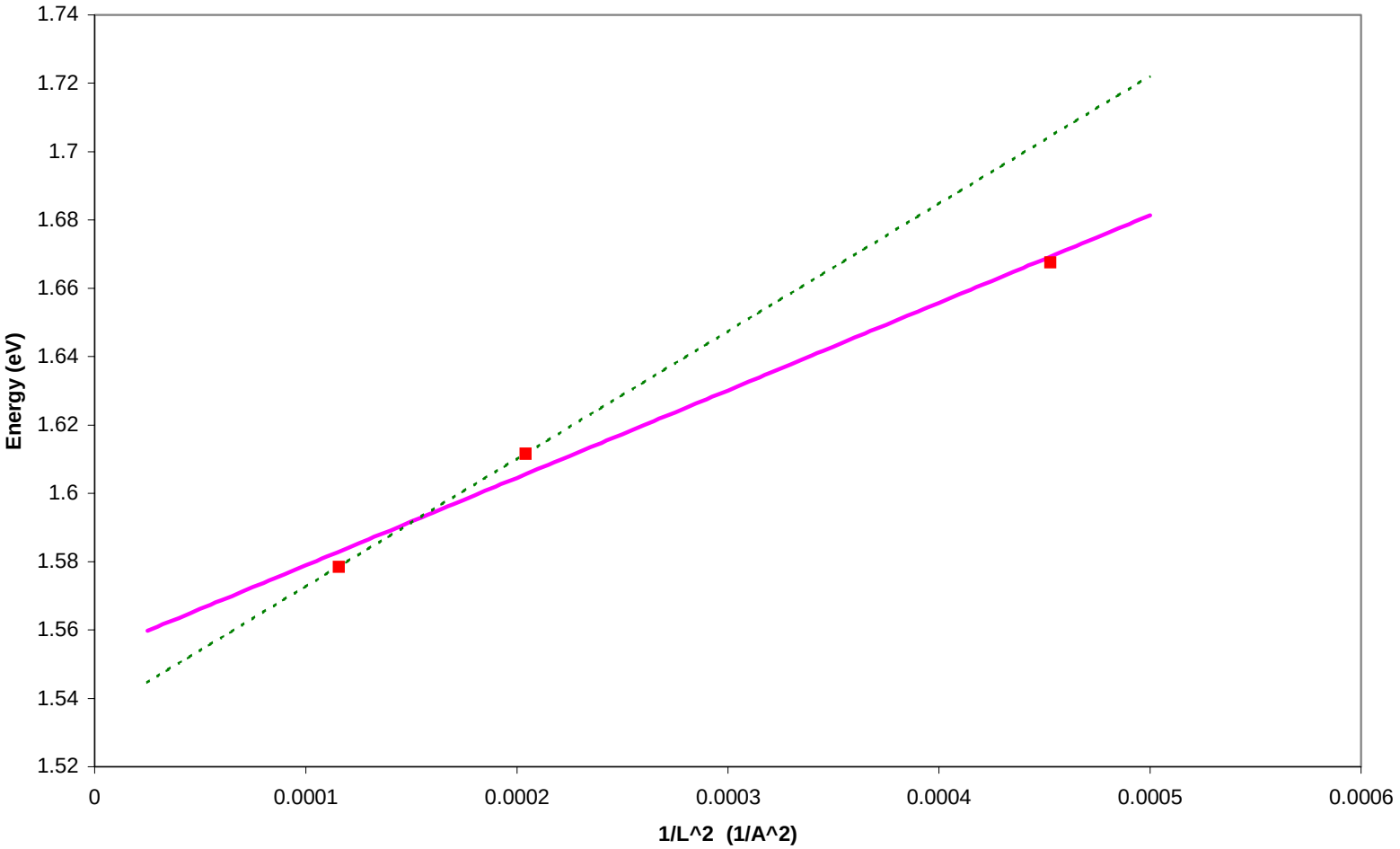
MQW E vs inv(1/L^2) T@ 75K light (47,70,93)
Energy (eV)
1.74
1.72
1.7
1.68
1.66
1.64
1.62
1.6
1.58
1.56
1.54
1.52
0
0.0001
0.0002
0.0003
0.0004
0.0005
0.0006
1/L^2 (1/A^2)

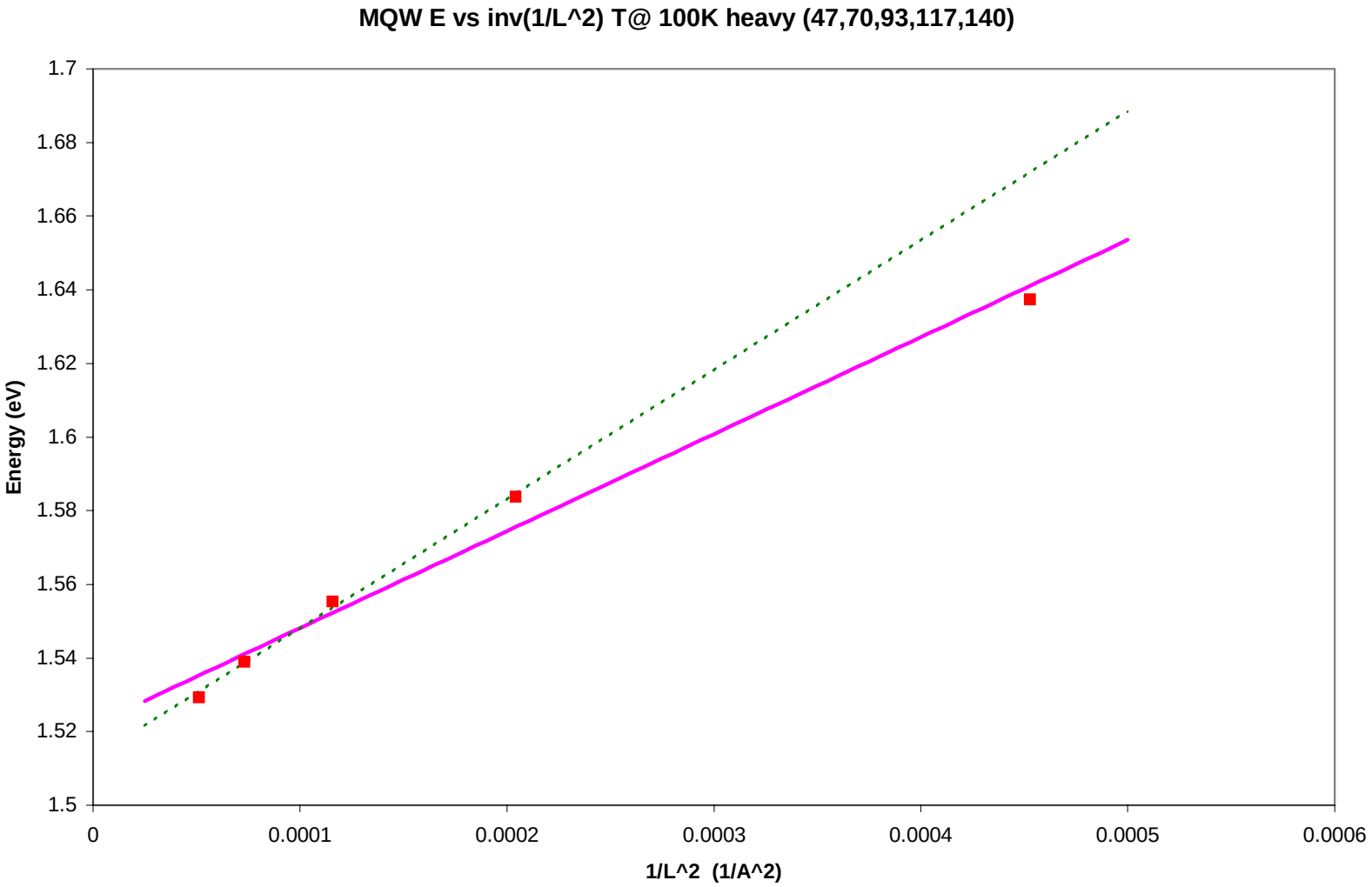
MQW E vs inv(1/L^2) T@ 100K heavy (47,70,93,117,140)
Energy (eV)
1.7
1.68
1.66
1.64
1.62
1.6
1.58
1.56
1.54
1.52
1.5
0
0.0001
0.0002
0.0003
0.0004
0.0005
0.0006
1/L^2 (1/A^2)

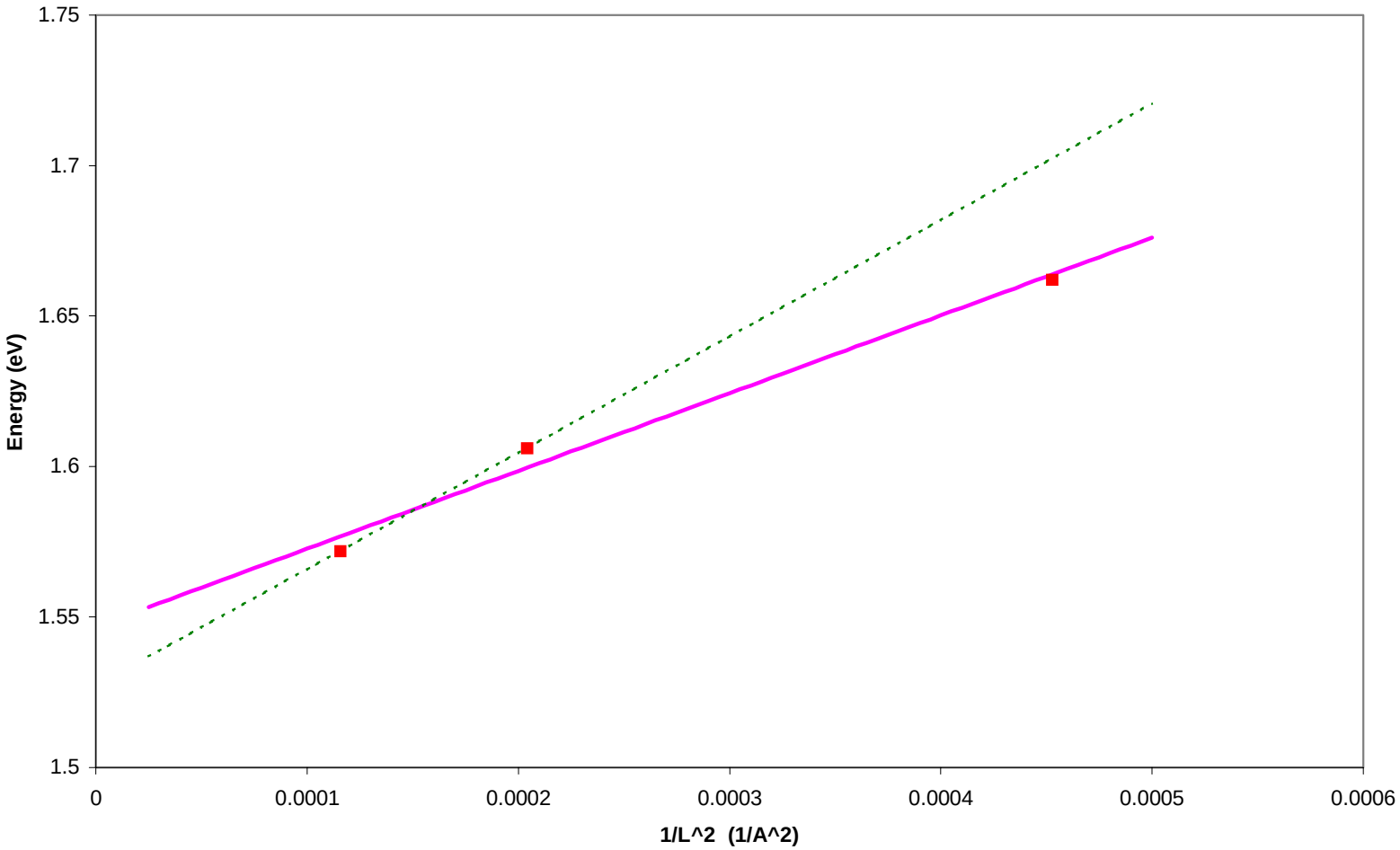
MQW E vs inv(1/L^2) T@ 100K light (47,70,93)
1.75
1.7
1.65
1.6
1.55
1.5
Energy (eV)
0
0.0001
0.0002
0.0003
0.0004
0.0005
0.0006
1/L^2 (1/A^2)

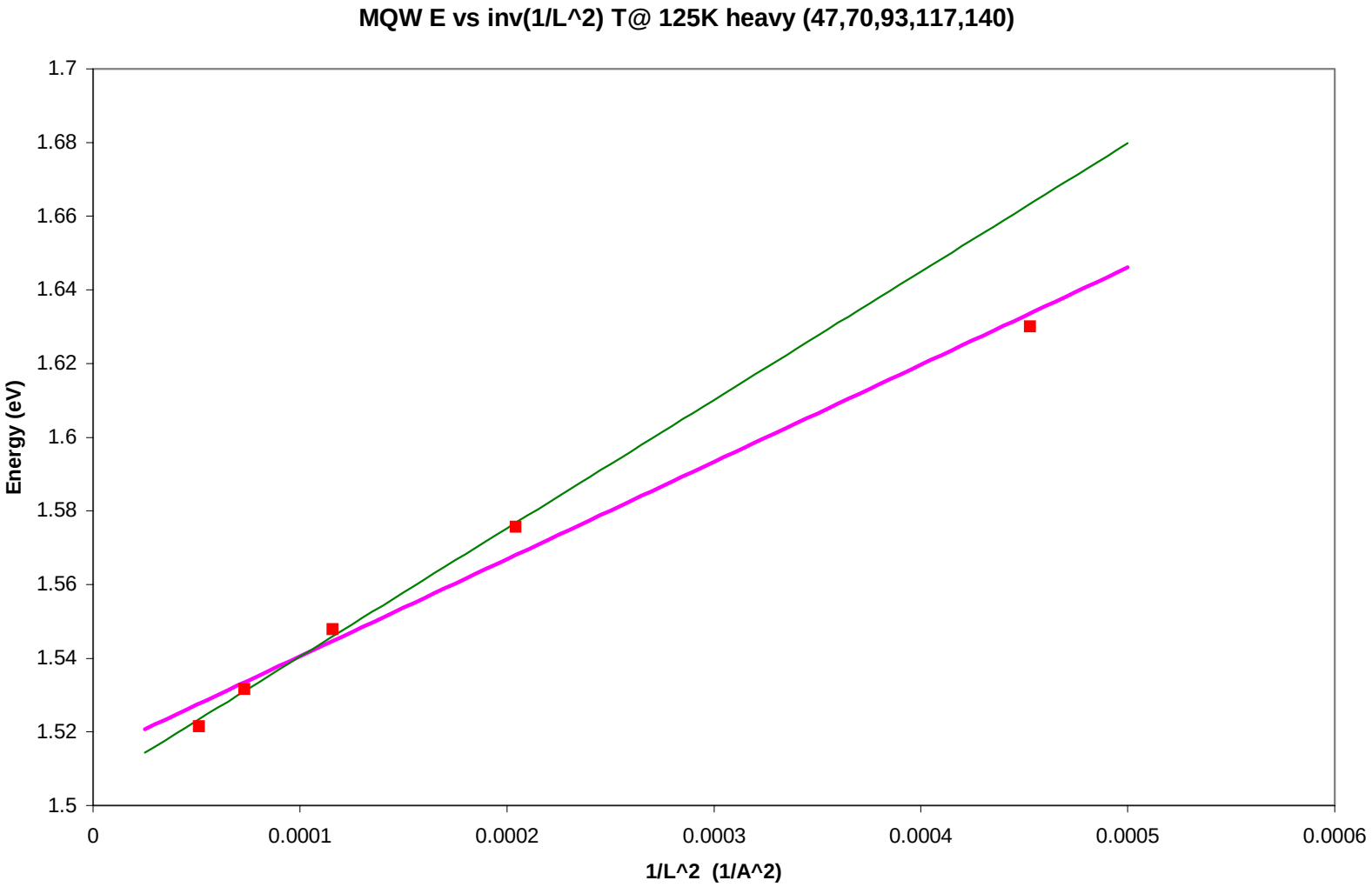
MQW E vs inv(1/L^2) T@ 125K heavy (47,70,93,117,140)
Energy (eV)
1.7
1.68
1.66
1.64
1.62
1.6
1.58
1.56
1.54
1.52
1.5
0
0.0001
0.0002
0.0003
0.0004
0.0005
0.0006
1/L^2 (1/A^2)

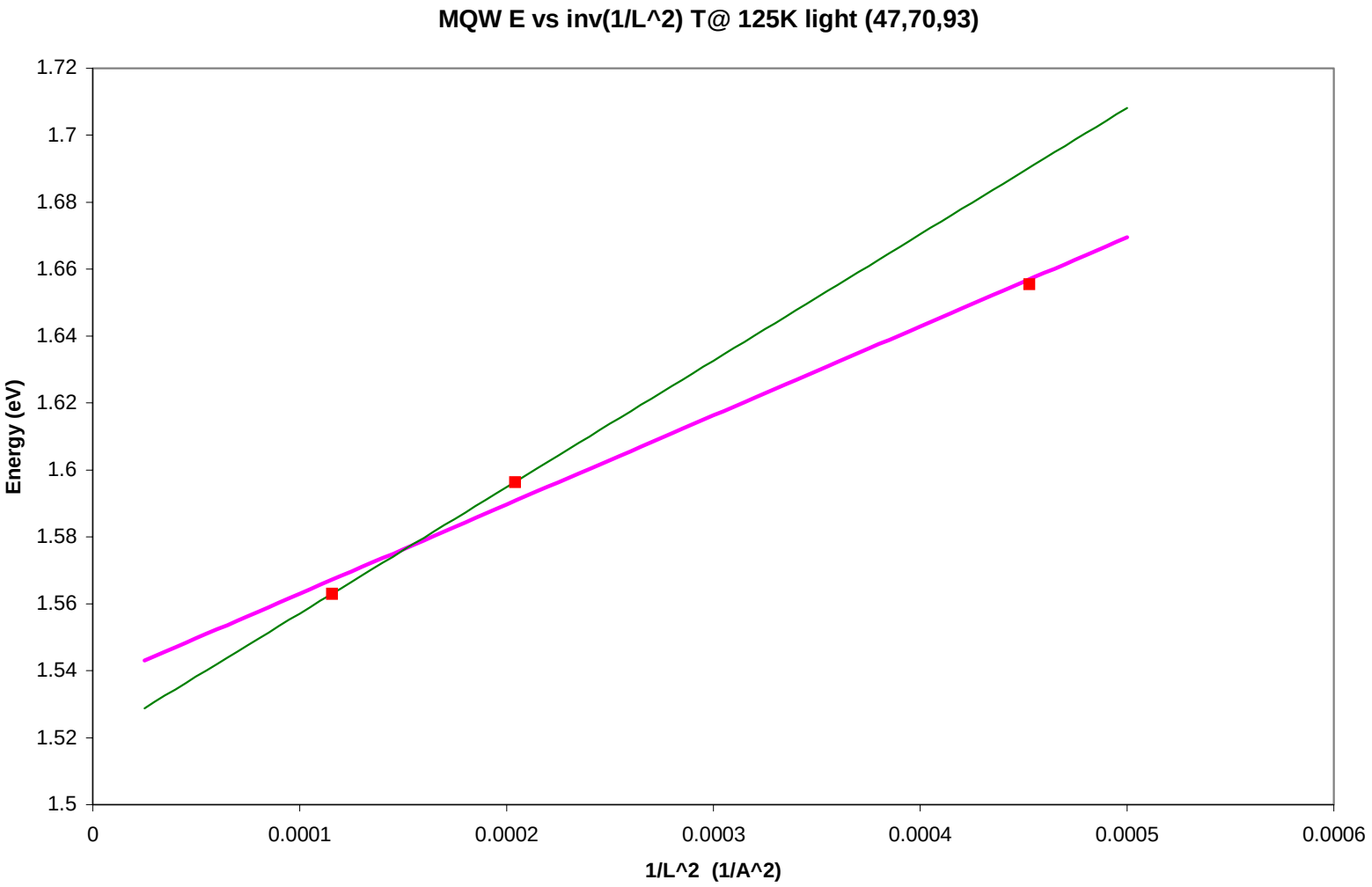
MQW E vs inv(1/L^2) T@ 125K light (47,70,93)
Energy (eV)
1.72
1.7
1.68
1.66
1.64
1.62
1.6
1.58
1.56
1.54
1.52
1.5
0
0.0001
0.0002
0.0003
0.0004
0.0005
0.0006
1/L^2 (1/A^2)

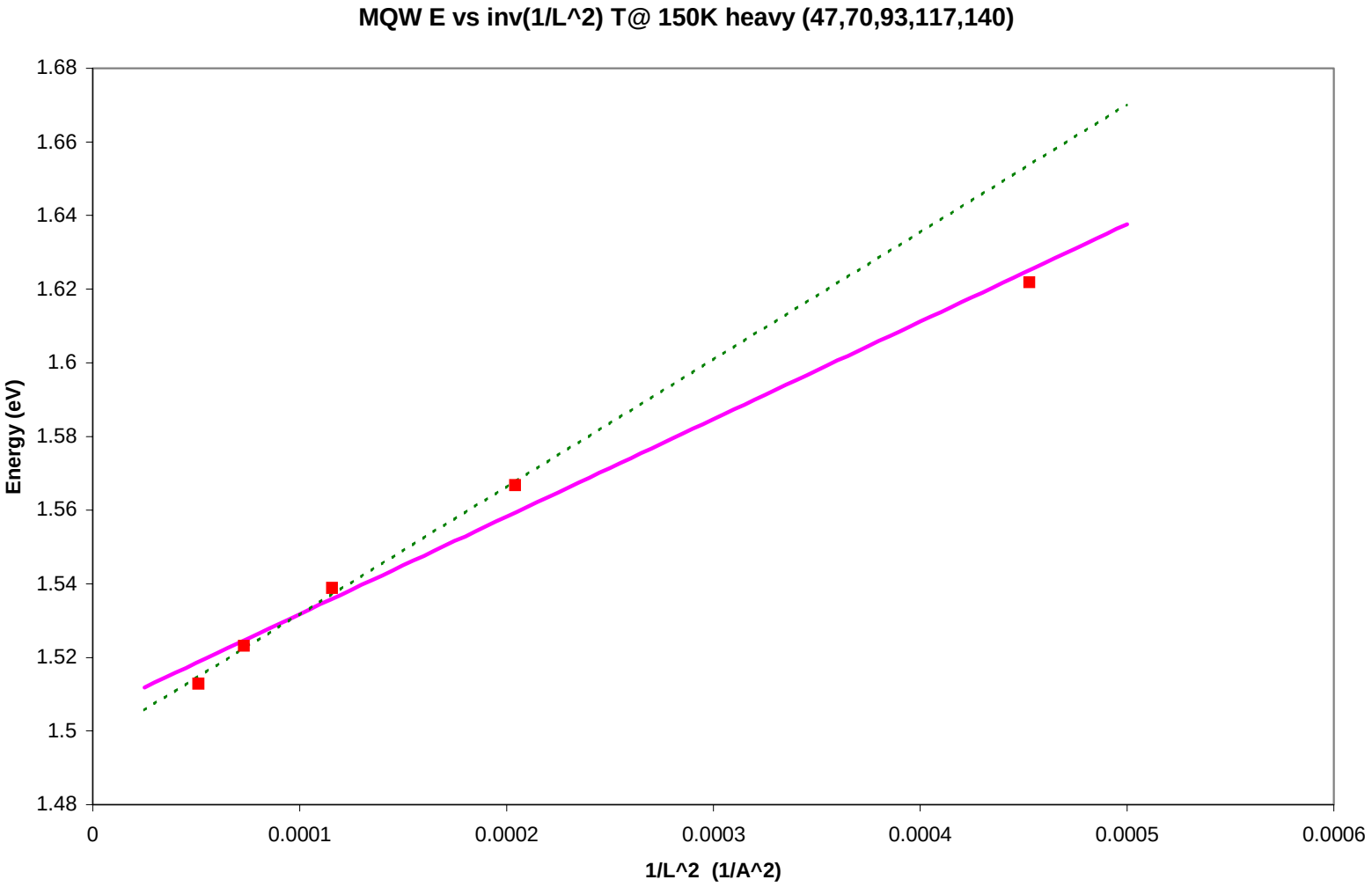
MQW E vs inv(1/L^2) T@ 150K heavy (47,70,93,117,140)
Energy (eV)
1.68
1.66
1.64
1.62
1.6
1.58
1.56
1.54
1.52
1.5
1.48
0
0.0001
0.0002
0.0003
0.0004
0.0005
0.0006
1/L^2 (1/A^2)

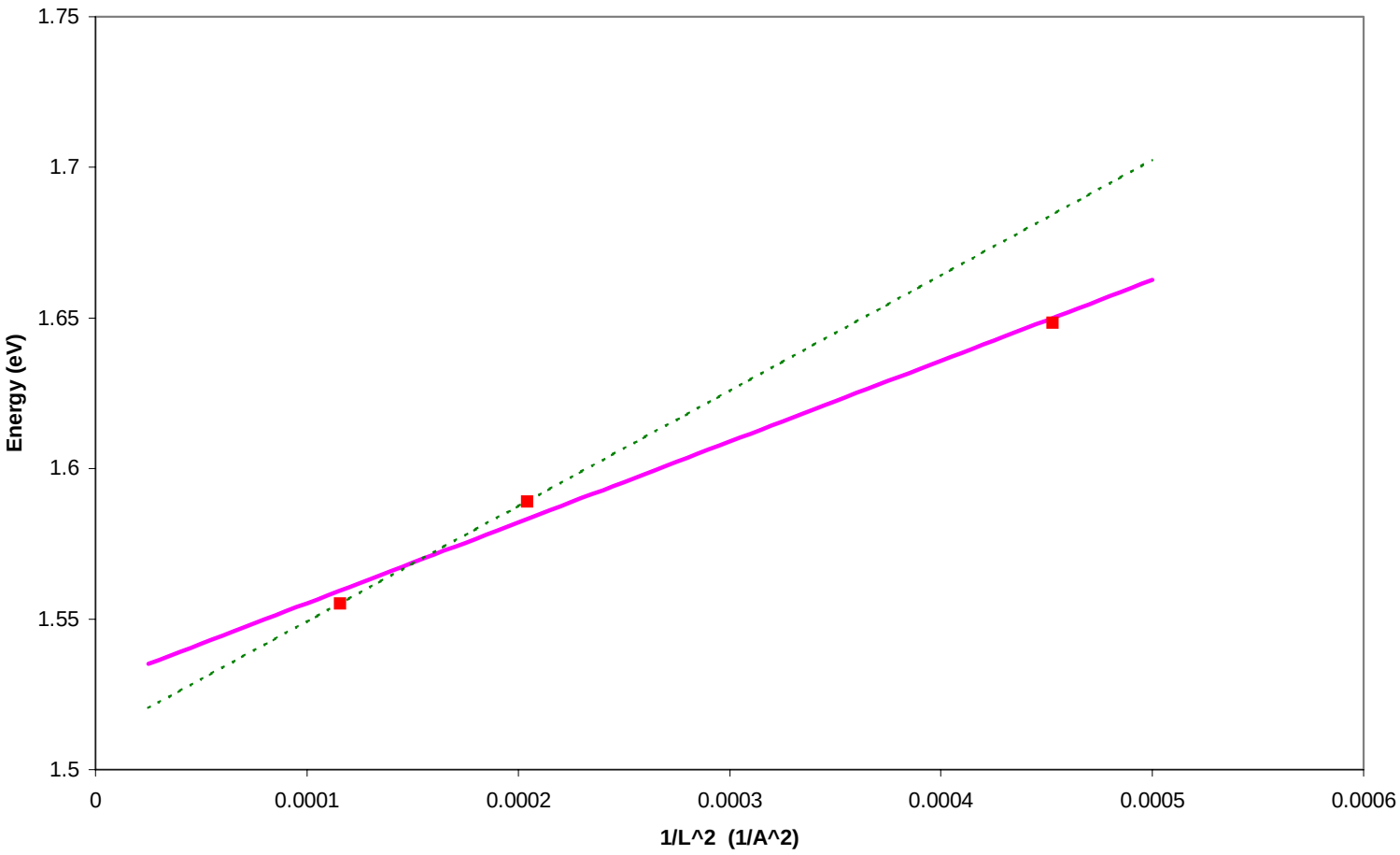
MQW E vs inv(1/L^2) T@ 150K light (47,70,93)
1.75
1.7
1.65
1.6
1.55
1.5
Energy (eV)
0
0.0001
0.0002
0.0003
0.0004
0.0005
0.0006
1/L^2 (1/A^2)

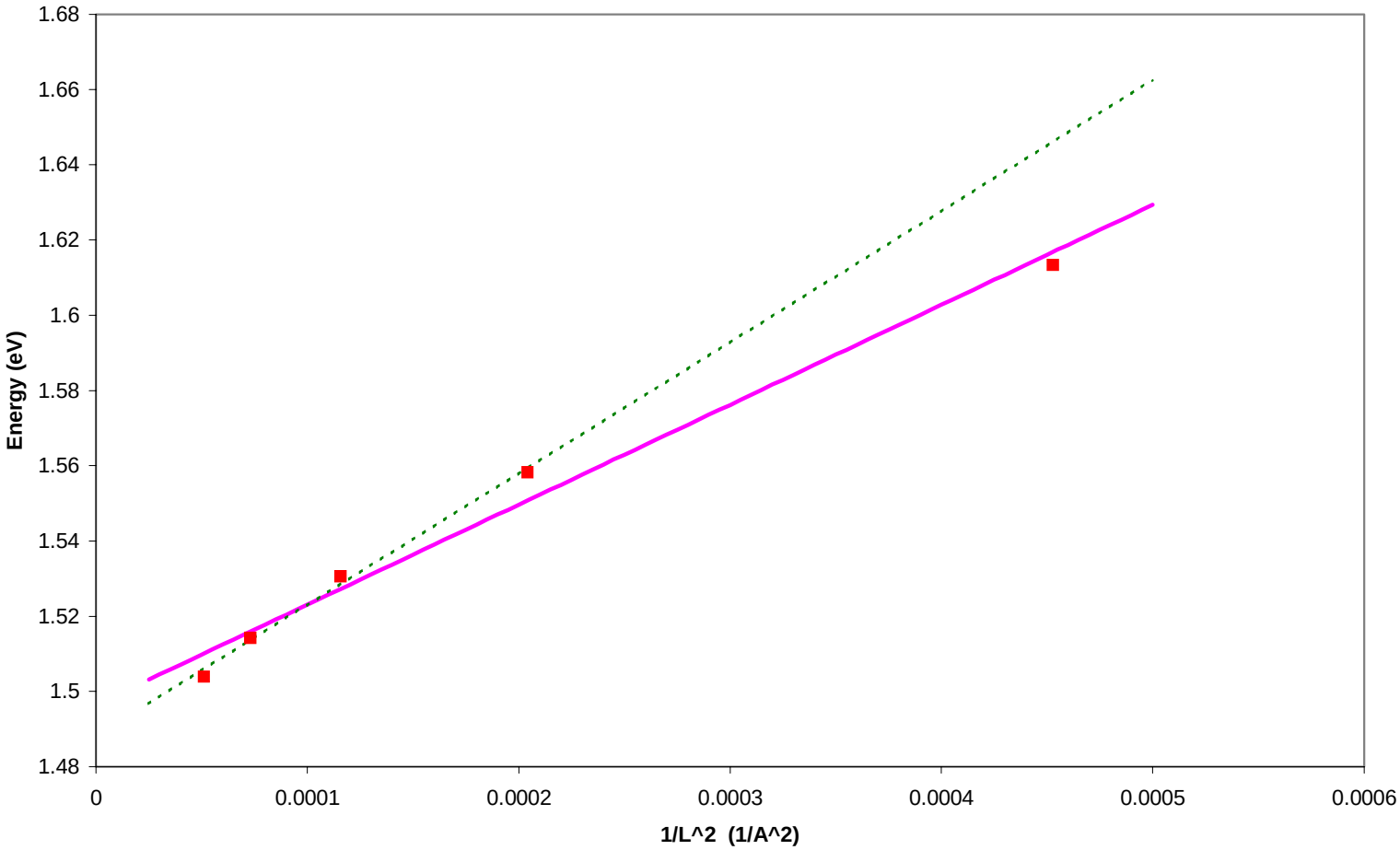
MQW E vs inv(1/L^2) T@ 175K heavy (47,70,93,117,140)
Energy (eV)
1.68
1.66
1.64
1.62
1.6
1.58
1.56
1.54
1.52
1.5
1.48
0
0.0001
0.0002
0.0003
0.0004
0.0005
0.0006
1/L^2 (1/A^2)

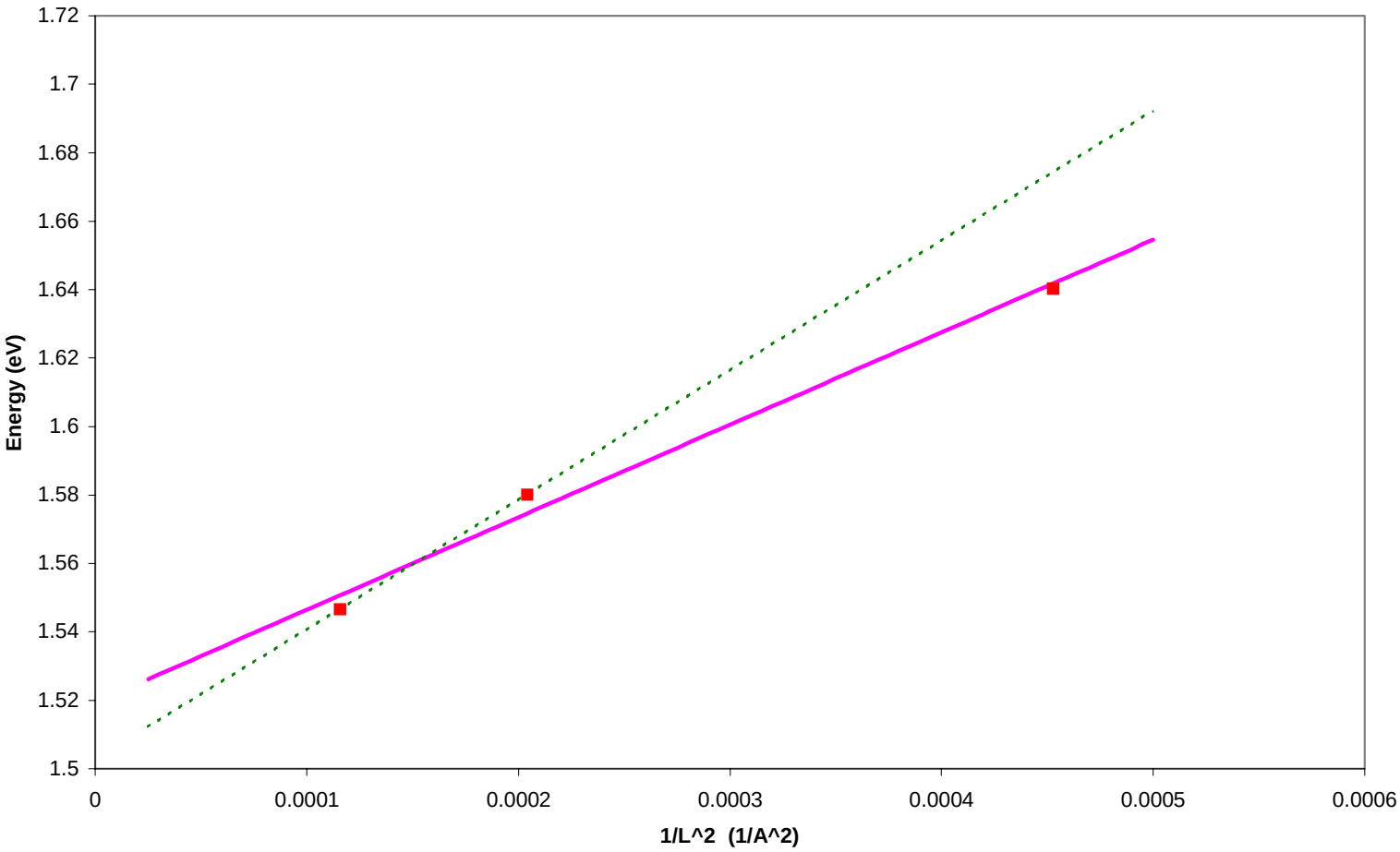
MQW E vs inv(1/L^2) T@ 175K light (47,70,93)
Energy (eV)
1.72
1.7
1.68
1.66
1.64
1.62
1.6
1.58
1.56
1.54
1.52
1.5
0
0.0001
0.0002
0.0003
0.0004
0.0005
0.0006
1/L^2 (1/A^2)

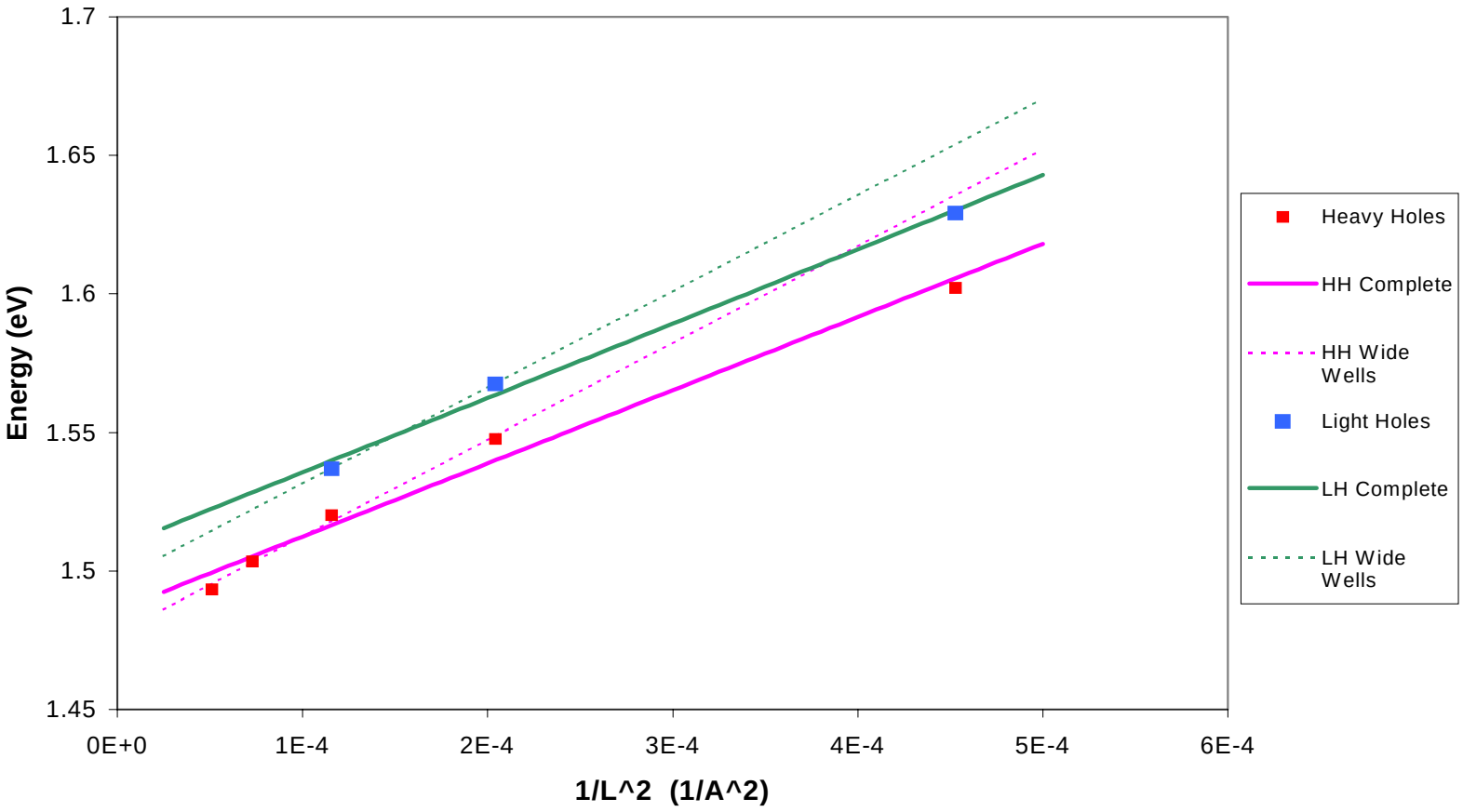
MQW E vs inv(1/L^2) T@ 200K:
Heavy (47,70,93,117,140); Light (47,70,93)
1.7
1.65
1.6
1.55
1.5
1.45
Energy (eV)
0E+0
1E-4
2E-4
3E-4
4E-4
5E-4
6E-4
1/L^2 (1/A^2)
Heavy Holes
HH Complete
HH Wide Wells
Light Holes
LH Complete
LH Wide Wells

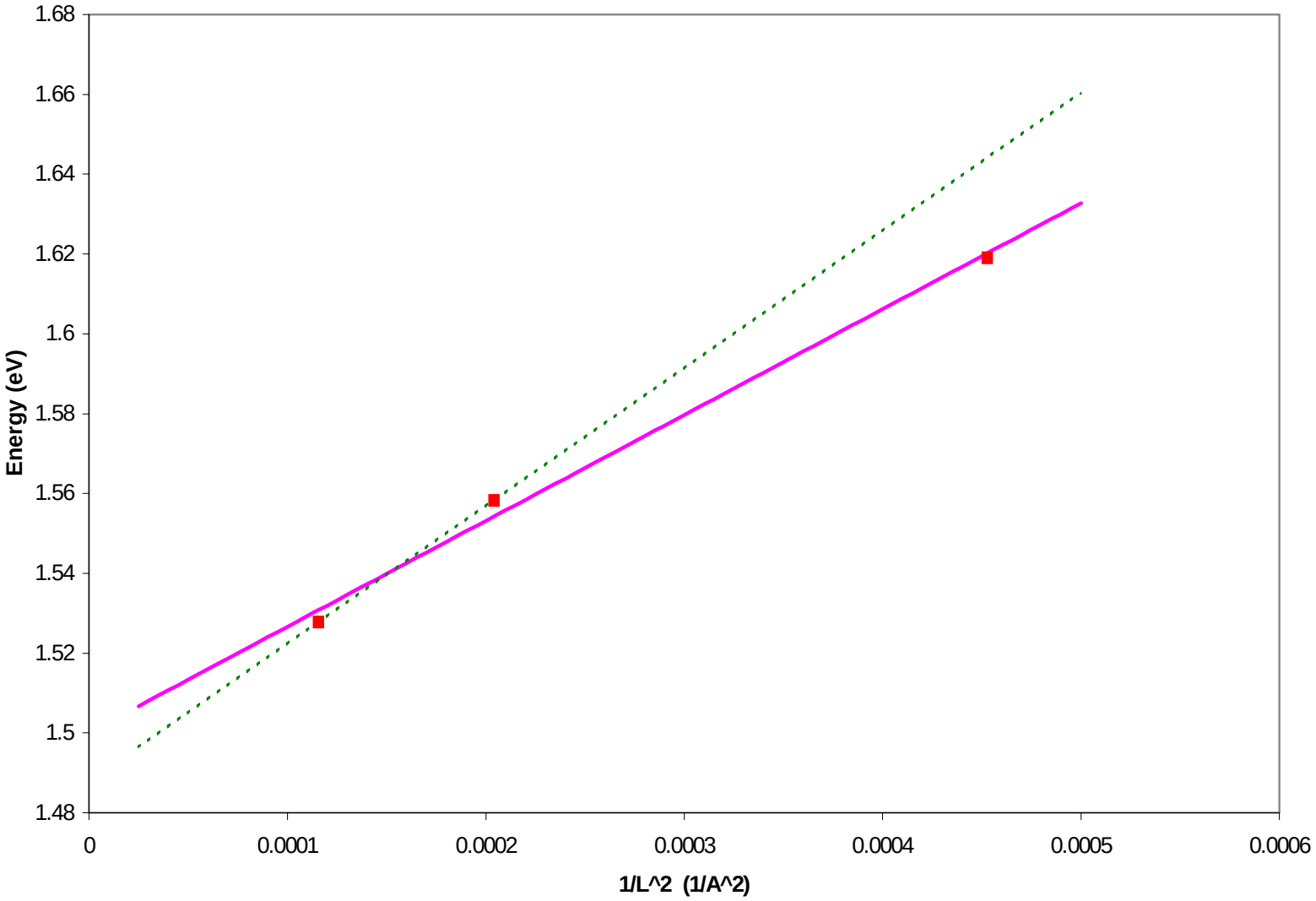
MQW E vs inv(1/L^2) T@ 220K light (47,70,93)
Energy (eV)
1.68
1.66
1.64
1.62
1.6
1.58
1.56
1.54
1.52
1.5
1.48
0
0.0001
0.0002
0.0003
0.0004
0.0005
0.0006
1/L^2 (1/A^2)

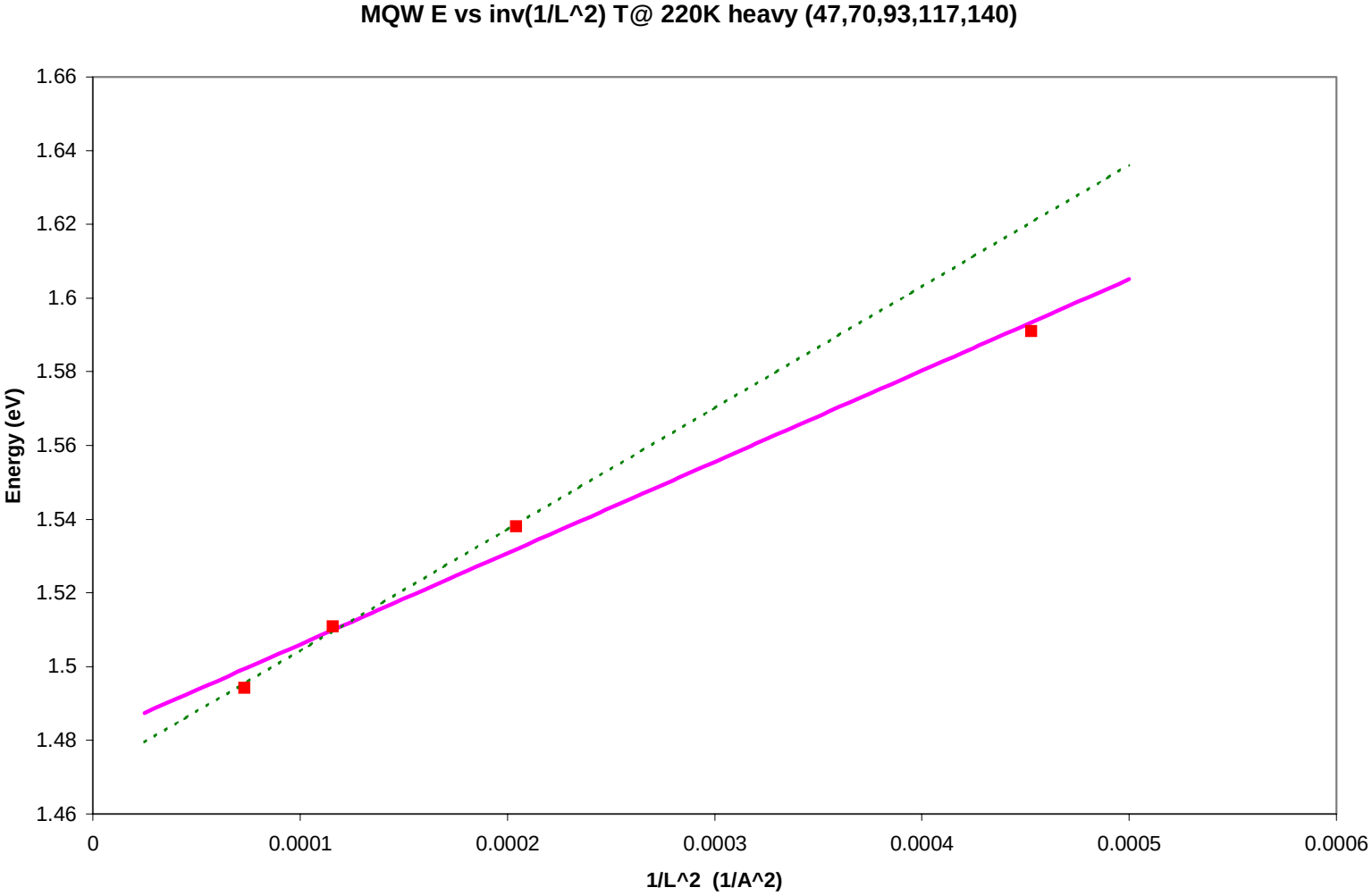
MQW E vs inv(1/L^2) T@ 220K heavy (47,70,93,117,140)
Energy (eV)
1.66
1.64
1.62
1.6
1.58
1.56
1.54
1.52
1.5
1.48
1.46
0
0.0001
0.0002
0.0003
0.0004
0.0005
0.0006
1/L^2 (1/A^2)

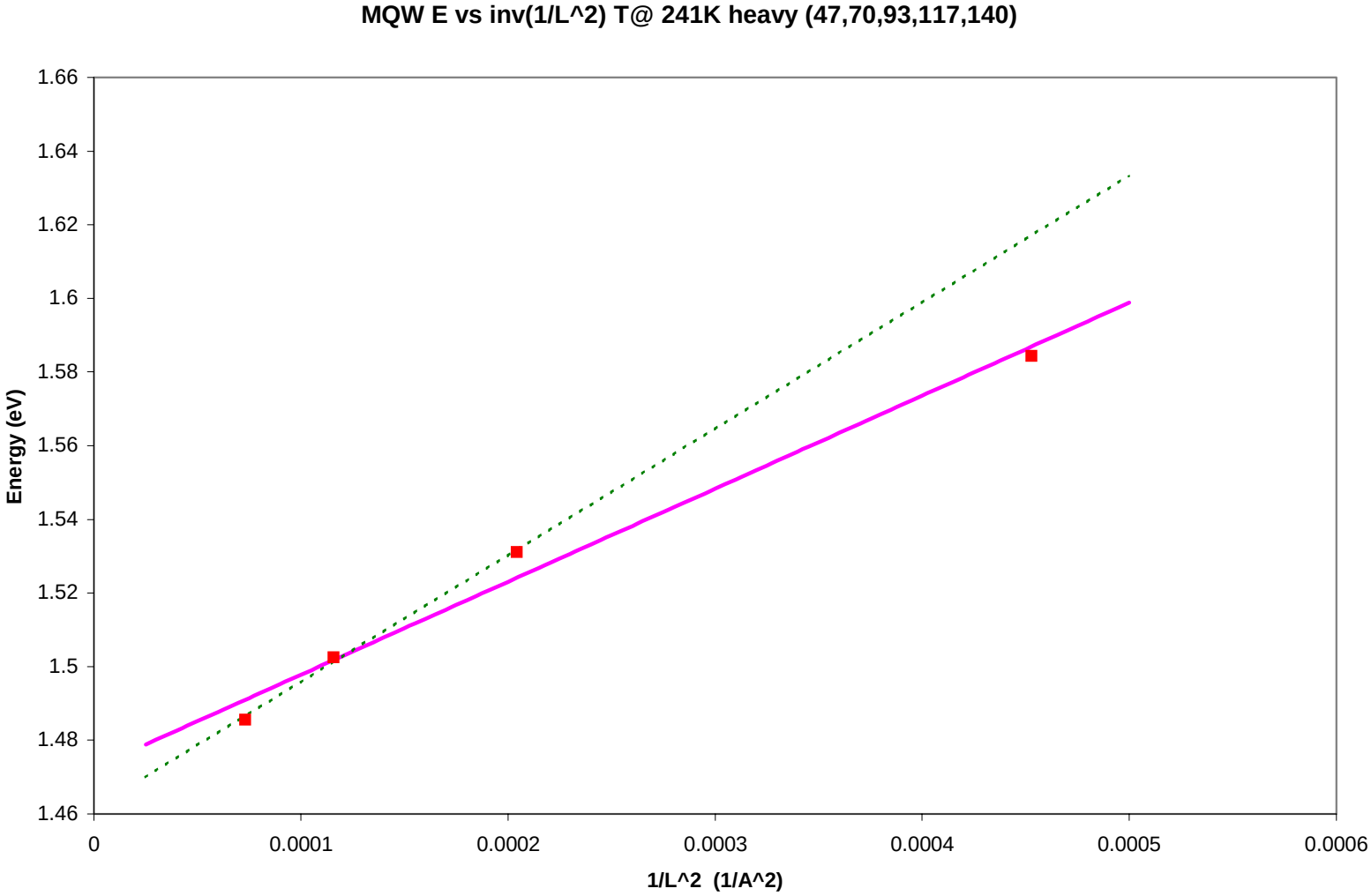
MQW E vs inv(1/L^2) T@ 241K heavy (47,70,93,117,140)
Energy (eV)
1.66
1.64
1.62
1.6
1.58
1.56
1.54
1.52
1.5
1.48
1.46
0
0.0001
0.0002
0.0003
0.0004
0.0005
0.0006
1/L^2 (1/A^2)

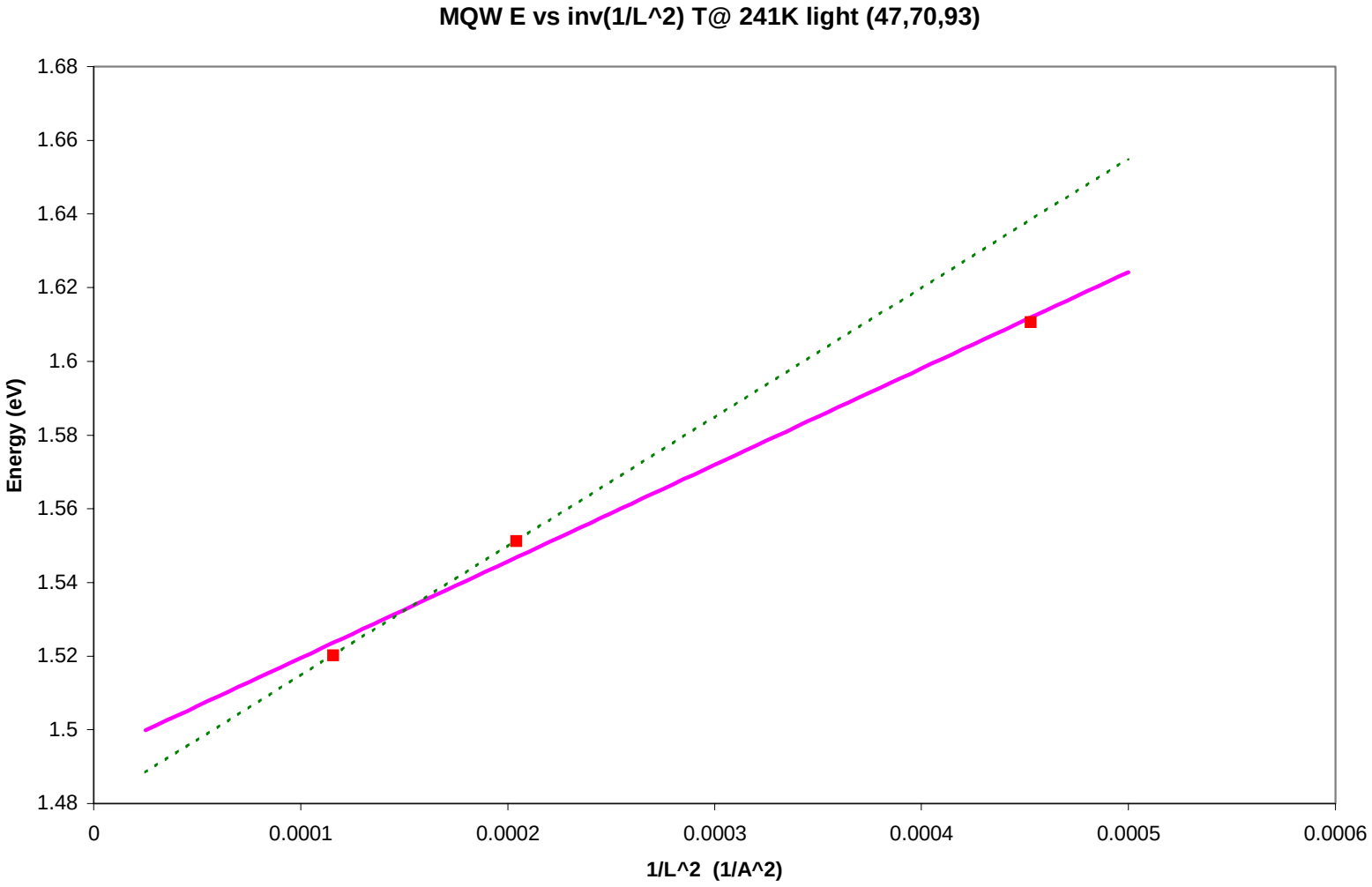
MQW E vs inv(1/L^2) T@ 241K light (47,70,93)
Energy (eV)
1.68
1.66
1.64
1.62
1.6
1.58
1.56
1.54
1.52
1.5
1.48
0
0.0001
0.0002
0.0003
0.0004
0.0005
0.0006
1/L^2 (1/A^2)

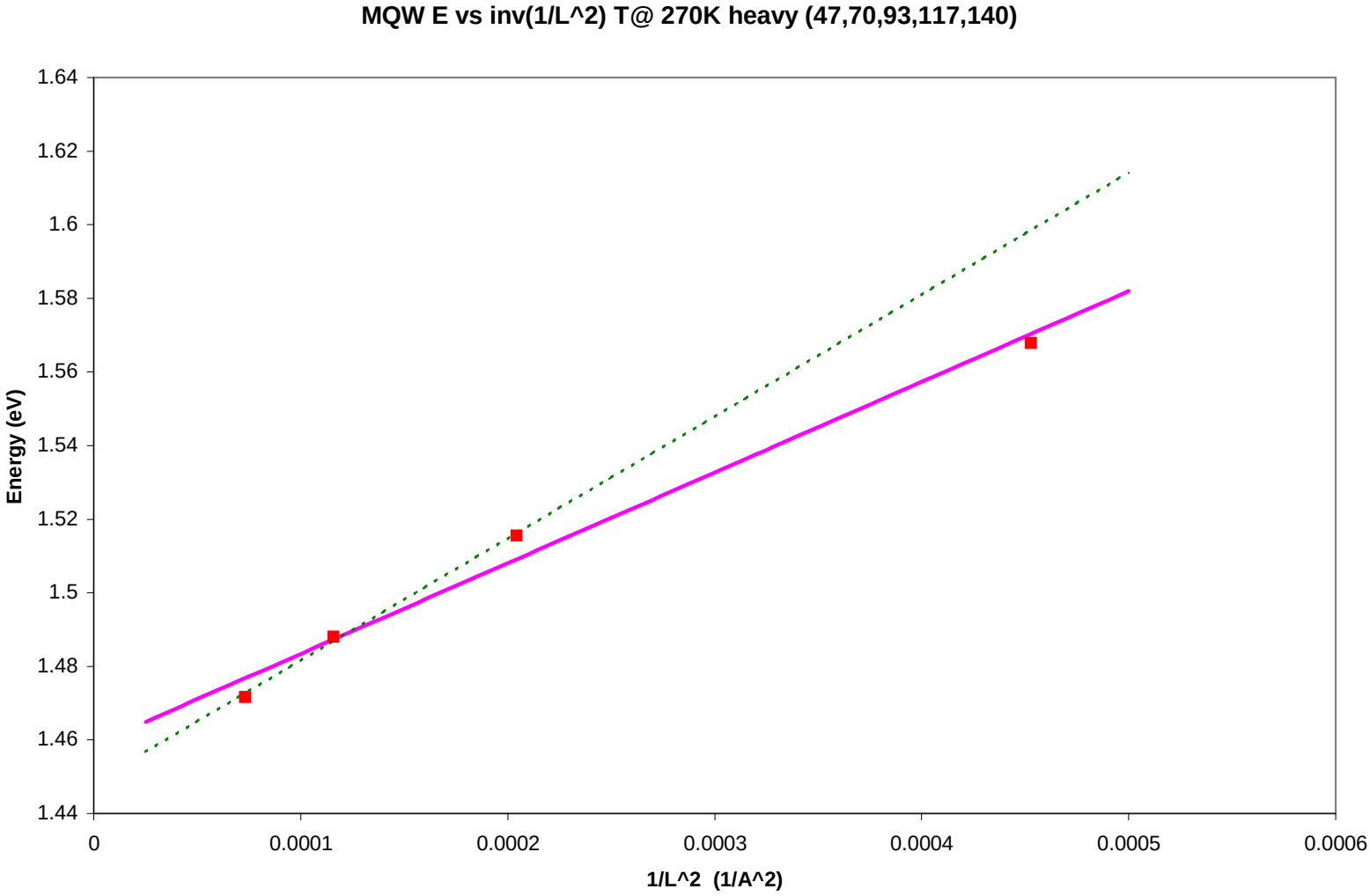
MQW E vs inv(1/L^2) T@ 270K heavy (47,70,93,117,140)
Energy (eV)
1.64
1.62
1.6
1.58
1.56
1.54
1.52
1.5
1.48
1.46
1.44
0
0.0001
0.0002
0.0003
0.0004
0.0005
0.0006
1/L^2 (1/A^2)

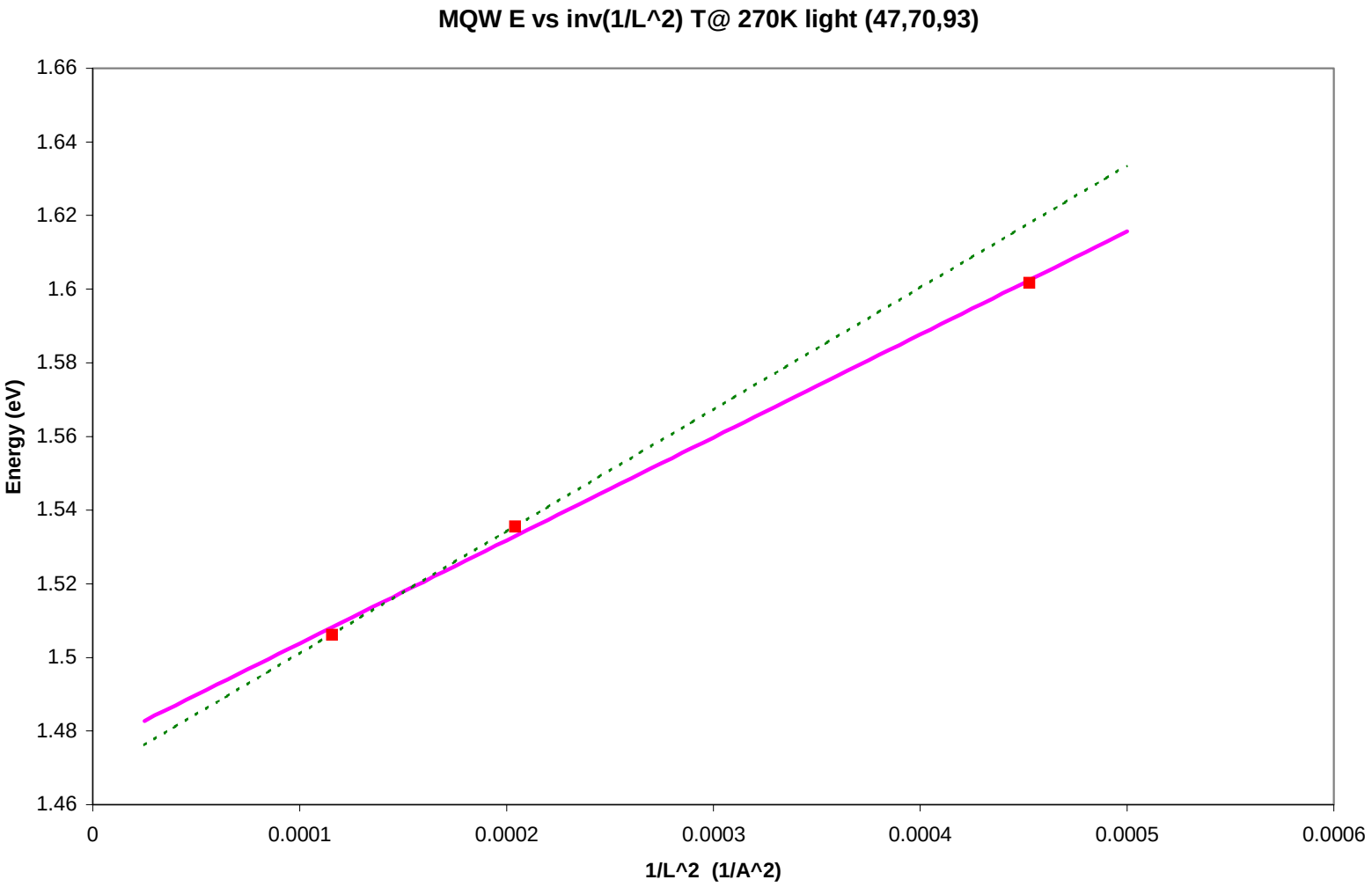
MQW E vs inv(1/L^2) T@ 270K light (47,70,93)
Energy (eV)
1.66
1.64
1.62
1.6
1.58
1.56
1.54
1.52
1.5
1.48
1.46
0
0.0001
0.0002
0.0003
0.0004
0.0005
0.0006
1/L^2 (1/A^2)

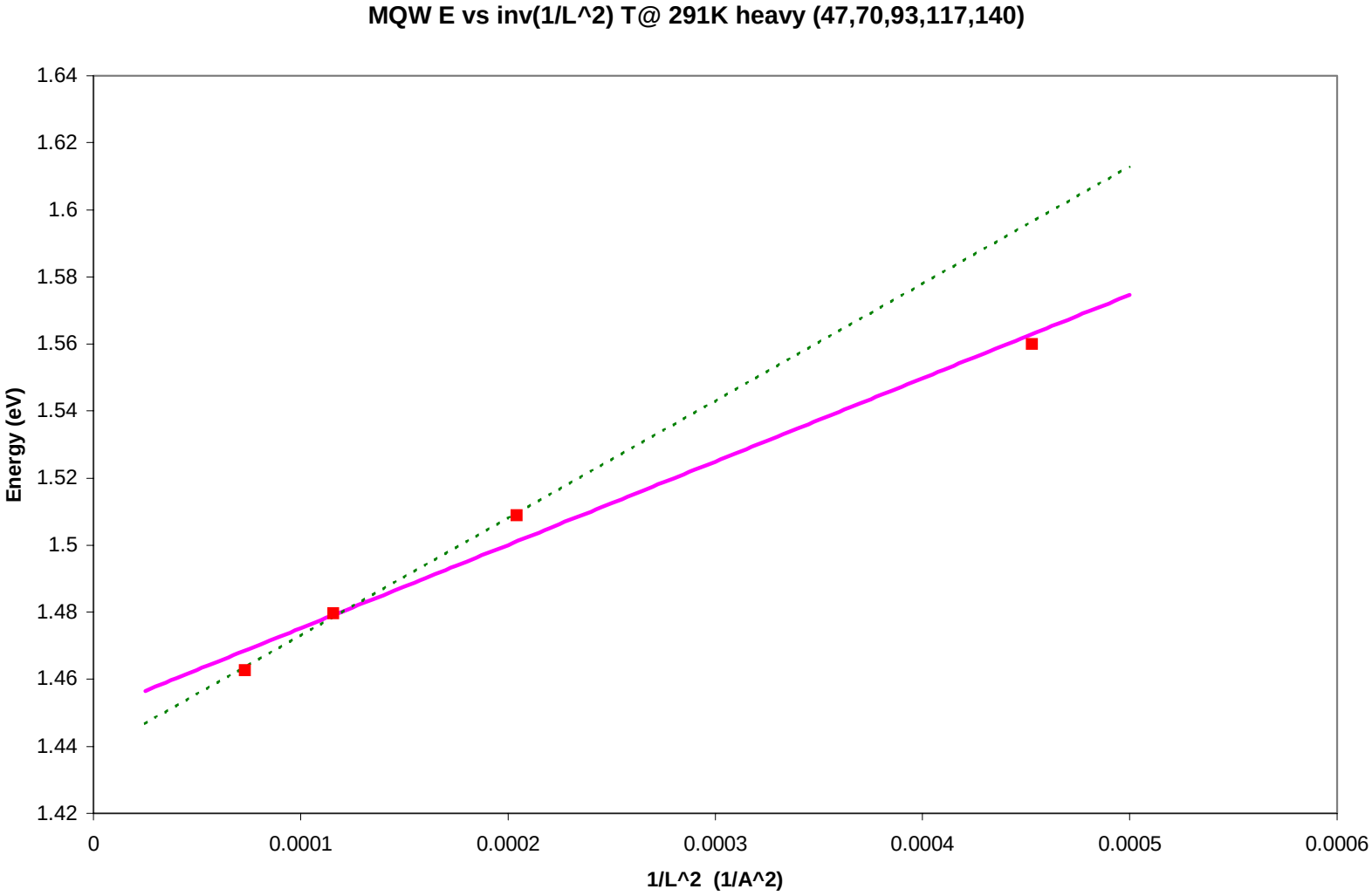
MQW E vs inv(1/L^2) T@ 291K heavy (47,70,93,117,140)
Energy (eV)
1.64
1.62
1.6
1.58
1.56
1.54
1.52
1.5
1.48
1.46
1.44
1.42
0
0.0001
0.0002
0.0003
0.0004
0.0005
0.0006
1/L^2 (1/A^2)

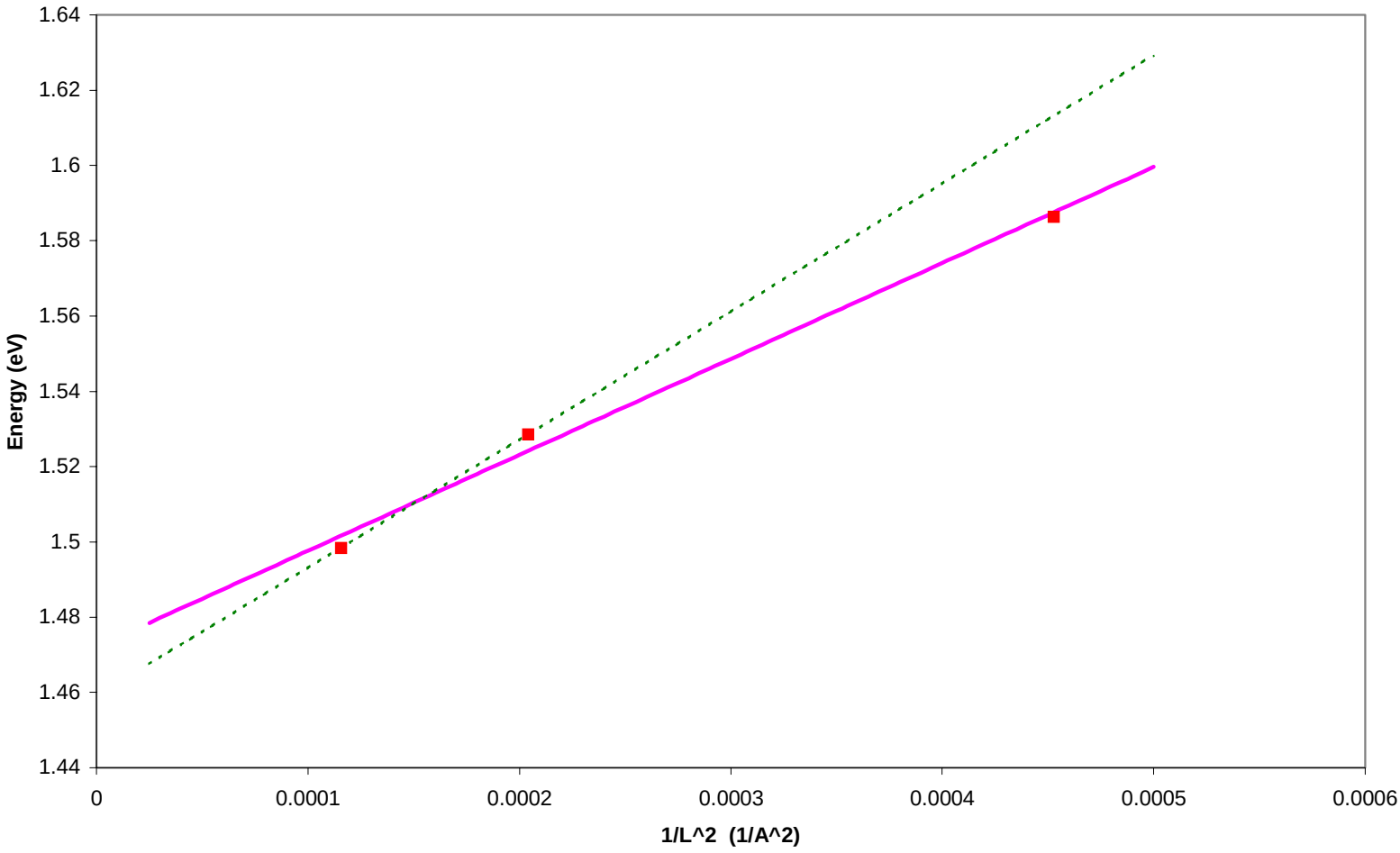
MQW E vs inv(1/L^2) T@ 291K light (47,70,93)
Energy (eV)
1.64
1.62
1.6
1.58
1.56
1.54
1.52
1.5
1.48
1.46
1.44
0
0.0001
0.0002
0.0003
0.0004
0.0005
0.0006
1/L^2 (1/A^2)

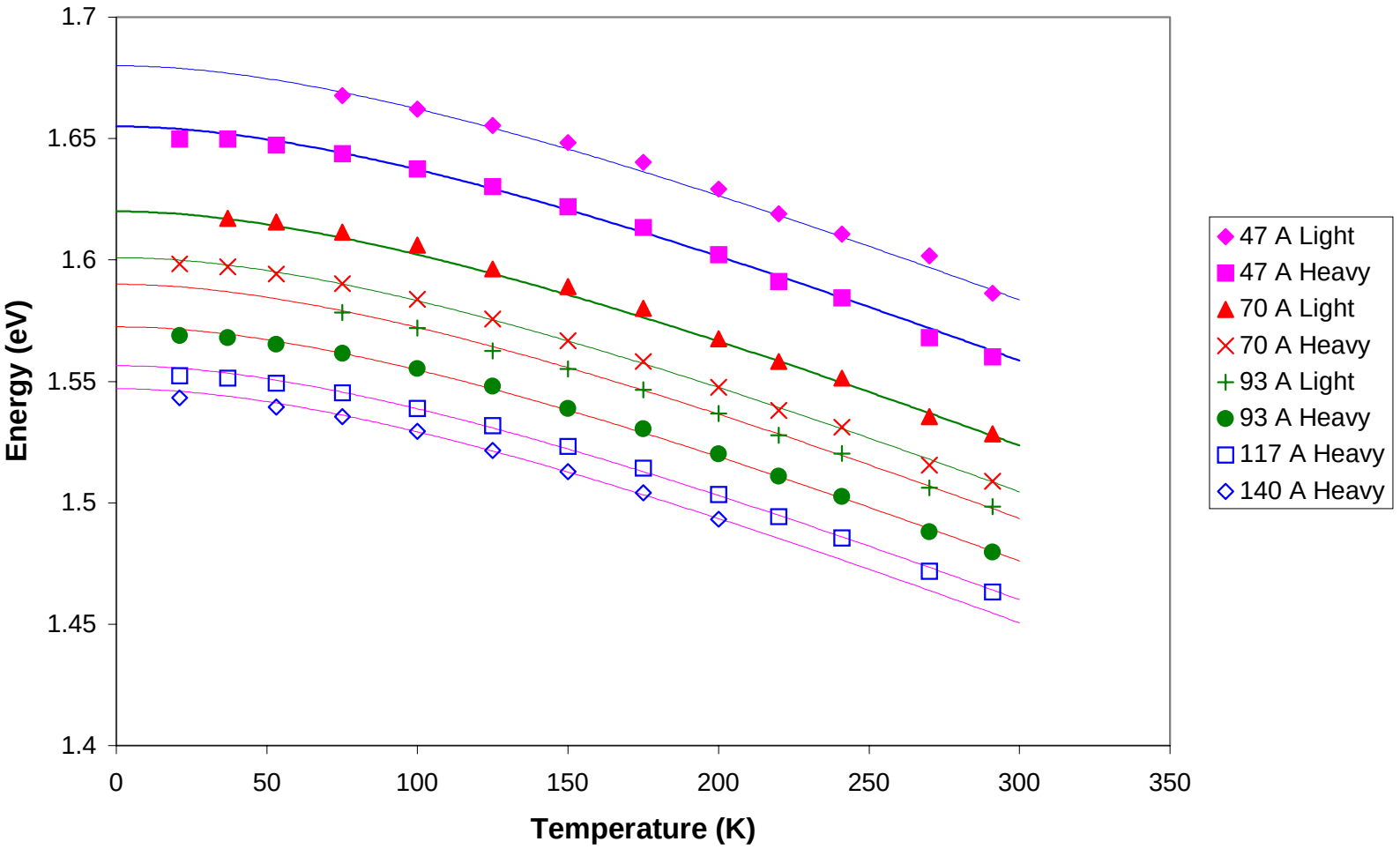
MQW Energy (eV) vs. Temperature (K) : Light and Heavy Holes
Energy (eV)
1.7
1.65
1.6
1.55
1.5
1.45
1.4
0
50
100
150
200
250
300
350
Temperature (K)
47 A Light
47 A Heavy
70 A Light
70 A Heavy
93 A Light
93 A Heavy
117 A Heavy
140 A Heavy